Eur. Phys. J. C (2019) 79:617
https://doi.org/10.1140/epjc/s10052-019-7114-8

THE EUROPEAN PHYSICAL JOURNAL C

Regular Article - Theoretical Physics

MSSM Higgs boson searches at the LHC: benchmark scenarios for Run 2 and beyond

Emanuele Bagnaschi[1], Henning Bahl[2], Elina Fuchs[3], Thomas Hahn[2], Sven Heinemeyer[4,5,6], Stefan Liebler[7], Shruti Patel[7,8], Pietro Slavich[9,a], Tim Stefaniak[10], Carlos E. M. Wagner[11,12,13], Georg Weiglein[10]

[1] Paul Scherrer Institute, 5232 Villigen, Switzerland
[2] Max-Planck Institut für Physik, 80805 Munich, Germany
[3] Department of Particle Physics and Astrophysics, Weizmann Institute of Science, 76100 Rehovot, Israel
[4] Instituto de Física de Cantabria (CSIC-UC), 39005 Santander, Spain
[5] Instituto de Física Teórica, (UAM/CSIC), Universidad Autónoma de Madrid, Cantoblanco, 28049 Madrid, Spain
[6] Campus of International Excellence UAM+CSIC, Cantoblanco, 28049 Madrid, Spain
[7] Institute for Theoretical Physics (ITP), Karlsruhe Institute of Technology, 76131 Karlsruhe, Germany
[8] Institute for Nuclear Physics (IKP), Karlsruhe Institute of Technology, 76344 Karlsruhe, Germany
[9] Laboratoire de Physique Théorique et Hautes Énergies, Sorbonne Université, CNRS, LPTHE, 75005 Paris, France
[10] DESY, Notkestraße 85, 22607 Hamburg, Germany
[11] High Energy Physics Division, Argonne National Laboratory, Argonne, IL 60439, USA
[12] Enrico Fermi Institute, University of Chicago, Chicago, IL 60637, USA
[13] Kavli Institute for Cosmological Physics, University of Chicago, Chicago, IL 60637, USA

Received: 4 October 2018 / Accepted: 8 July 2019 / Published online: 20 July 2019

Abstract We propose six new benchmark scenarios for Higgs boson searches in the Minimal Supersymmetric Standard Model. Our calculations follow the recommendations of the LHC Higgs Cross Section Working Group, and benefit from recent developments in the predictions for the Higgs-boson masses and mixing. All of the proposed scenarios are compatible with the most recent results from Run 2 of the LHC. In particular, they feature a scalar with mass and couplings compatible with those of the observed Higgs boson, and a significant portion of their parameter space is allowed by the limits from the searches for SUSY particles and additional Higgs bosons. We define a scenario where all SUSY particles are relatively heavy, and two scenarios with light colorless SUSY particles (charginos, neutralinos and, in one case, staus). In addition, we present two scenarios featuring alignment without decoupling, realized with either the lighter or the heavier scalar being SM-like, and a scenario with $\mathcal{CP}$ violation.

1 Introduction

In the six years since the discovery of a Higgs boson at the LHC [1,2], its mass has been measured with a few-per-mil accuracy, $M_H^{\rm obs} = 125.09 \pm 0.24$ GeV [3]. The measured properties are, within current experimental and theoretical uncertainties, in agreement with the predictions of the Standard Model (SM) [4]. Together with the current lack of discoveries of beyond-the-SM (BSM) particles at the LHC with center-of-mass energies of up to 13 TeV, the requirement that the particle spectrum include an essentially SM-like Higgs boson imposes important constraints on the parameter space of possible extensions of the SM.

The Minimal Supersymmetric Standard Model (MSSM) [5–7] is one of the best motivated among those extensions – and probably the most studied. Its Higgs sector consists of two SU(2) doublets, H_1 and H_2, whose relative contribution to electroweak symmetry breaking (EWSB) is determined by the ratio of vacuum expectation values (vevs) of their neutral components, $\tan\beta \equiv v_2/v_1$. At the tree level, $\mathcal{CP}$ is conserved in the Higgs sector of the MSSM, and the spectrum of physical Higgs bosons consists of two neutral $\mathcal{CP}$-even scalars, of which we denote the lighter as h and the heavier as H, one $\mathcal{CP}$-odd scalar, A, and a charged-scalar pair, $H^\pm$. Supersymmetry (SUSY) imposes relations between the quartic Higgs couplings and the gauge couplings, ensuring that the tree-level masses of all Higgs bosons can be expressed in terms of the gauge-boson masses, M_Z and M_W, plus two additional parameters which can be chosen as the $\mathcal{CP}$-odd scalar mass, M_A (or alternatively the charged Higgs boson mass, $M_{H^\pm}$), and $\tan\beta$. In particular, the tree-level mass of the lighter $\mathcal{CP}$-even scalar h is bounded from above

[a] e-mail: slavich@lpthe.jussieu.fr

by $M_Z\,|\cos 2\beta|$. However, radiative corrections – especially those involving top and bottom quarks and their scalar partners, the stops and the sbottoms – can significantly alter the tree-level predictions for the Higgs masses, allowing for $M_h \approx 125$ GeV but bringing along a dependence on many free parameters of the MSSM, see Ref. [8] for a recent review. Moreover, for specific choices of those parameters, radiative corrections to the mixing between the scalars can also allow for scenarios in which the heavier mass eigenstate, H, is the one with $M_H \approx 125$ GeV and roughly SM-like couplings, see e.g. Refs. [9–12]. In the presence of complex parameters in the MSSM Lagrangian, radiative corrections can break $\mathcal{CP}$ in the Higgs sector and induce a mixing among the two $\mathcal{CP}$-even scalars, h and H, and the $\mathcal{CP}$-odd scalar, A, such that beyond tree-level they combine into three neutral mass eigenstates which we denote as h_a (with $a = 1, 2, 3$).

The large number of free parameters complicates the task of interpreting within the MSSM both the properties of the observed Higgs boson and the results of the ongoing searches for additional, non-standard Higgs bosons. Complete scans of the MSSM parameter space would be highly impractical for experimental analyses and phenomenological studies. Therefore, a number of *benchmark scenarios* has been proposed over the years, for both the $\mathcal{CP}$-conserving [13–15] and $\mathcal{CP}$-violating [16,17] cases. In these scenarios, two parameters in the Higgs sector are varied – typically, one of them is $\tan\beta$ and the other is either M_A, for the $\mathcal{CP}$-conserving case, or $M_{H^\pm}$, for the $\mathcal{CP}$-violating case – while the remaining parameters (such as the soft-SUSY-breaking masses and mixing terms for the sfermions, as well as the masses of gauginos and higgsinos) are fixed to values chosen to exhibit certain aspects of MSSM Higgs phenomenology. In particular, Ref. [15] proposed seven $\mathcal{CP}$-conserving benchmark scenarios that, over a wide range of values of the two free parameters, featured a Higgs boson whose properties were compatible with those measured during Run 1 of the LHC. Three of those scenarios involved relatively heavy colored superpartners, with masses of the order of one TeV, and lighter charginos and neutralinos with masses around 200 GeV or less; one scenario involved a light stop of mass about 325 GeV, with a "compressed" stop–neutralino spectrum to avoid the exclusion bounds from direct stop searches; one scenario involved a light stau, allowing for a sizable contribution to the diphoton width of the SM-like Higgs boson; in one scenario the radiative corrections to the Higgs mixing led to reduced couplings to down-type fermions; finally, in the last scenario the heavier $\mathcal{CP}$-even scalar H could be identified with the observed Higgs boson.

The LHC Higgs Cross Section Working Group (LHC-HXSWG) produced a set of `ROOT` files [18,19] providing, for each of the benchmark scenarios of Ref. [15], what were then state-of-the-art predictions for the masses, production cross sections and decay widths of the three neutral Higgs bosons, over a grid of values of M_A and $\tan\beta$ (except for the last scenario, in which the free parameters are $\tan\beta$ and the Higgs/higgsino superpotential mass μ). Those predictions were subsequently used by both the ATLAS and CMS collaborations to interpret the results of their searches for additional scalars in the context of the MSSM.

Important developments in the years since the publication of Ref. [15] motivate a reassessment of the benchmark scenarios presented there. On the one hand, the full analysis of Run-1 LHC data at center-of-mass energies of 7 and 8 TeV, as well as the available analyses of Run-2 data at 13 TeV, have tightened the experimental constraints on masses and couplings of both the observed Higgs boson and any still-unobserved BSM particles. On the other hand, the theoretical predictions for the MSSM Higgs-boson masses have evolved: the renewed interest in SUSY scenarios with heavy superpartners (i.e., with masses larger than a few TeV) has stimulated new calculations [20–31] aiming at the resummation of potentially large corrections enhanced by logarithms of the ratio between the SUSY scale and the EWSB scale. The versions of the code `FeynHiggs` [32] used both to devise the scenarios of Ref. [15] and in the production of the corresponding LHC-HXSWG files relied on a fixed-order calculation of the MSSM Higgs masses, employing full one-loop corrections from Ref. [33] and the dominant two-loop corrections from Refs. [34–38]. In contrast, newer versions of `FeynHiggs` include also a full next-to-leading-logarithmic (NLL) and partial next-to-NLL (NNLL) resummation of the large logarithmic corrections [20,24,28], based on an effective-field-theory (EFT) approach. Implementing this resummation required modifications in the code that, even for the stop masses around one TeV featured in the scenarios of Ref. [15], can lower the prediction for M_h by $1-2$ GeV. For an example of the combined effect of these developments, we can consider the case of the "light-stop" scenario of Ref. [15]: pair production of the lighter stop followed by the decay $\tilde{t}_1 \to c\,\tilde{\chi}_1^0$ is now excluded by monojet searches by ATLAS [39] and CMS [40] for stop masses of up to 430 GeV and 510 GeV, respectively, unless the lightest neutralino is so close in mass to the stop that the latter becomes long-lived. In addition, the lowering of the prediction for M_h in recent versions of `FeynHiggs` makes the "light-stop" scenario of Ref. [15] incompatible with an observed Higgs mass of about 125 GeV, even within a theoretical uncertainty usually estimated as ± 3 GeV [41,42].

For the MSSM with complex parameters, and thus a mixing among all three neutral Higgs states, benchmark scenarios were originally proposed in Ref. [16], to be used in the interpretation of the searches for MSSM Higgs bosons at LEP [43]. They were later updated in Ref. [17] to include a SM-like Higgs boson with mass around 125 GeV. In those papers, the masses and couplings of the Higgs bosons were computed with the code `CPsuperH` [44–46], relying on the

calculation of Refs. [47–49]. However, no scenario with $\mathcal{CP}$ violation in the Higgs sector has been considered so far in the context of the LHC-HXSWG. A reassessment of the benchmark scenarios for the MSSM with complex parameters seems now well motivated, in view of tightening constraints from electric dipole moments (EDMs) [50,51], as well as of recent progress in the calculation of the Higgs masses (allowing for complex phases in the dominant two-loop corrections [52–57] and, approximately, in the large-log resummation [28]), in the prediction of the cross sections for Higgs production [58] and in the incorporation of interference effects among admixed Higgs bosons [59–61].

Another type of MSSM benchmark scenarios that was studied by the LHC-HXSWG [62] is characterized by very low values of $\tan\beta$, and requires very heavy SUSY particles. Indeed, the tree-level MSSM prediction for M_h goes to zero as $\tan\beta$ approaches unity, thus, at very low $\tan\beta$, stop masses much larger than a few TeV are needed to obtain $M_h \approx 125$ GeV through radiative corrections. The precise calculation of the Higgs masses and couplings in these scenarios, including a proper resummation of large logarithmic corrections, requires an EFT approach in which the theory valid below the SUSY scale is a two-Higgs-doublet model (2HDM). Work in this direction has been presented in Refs. [63,64], and the setup with heavy SUSY and a light 2HDM is also being implemented in `FeynHiggs` [65]. In this paper, however, we will focus on benchmark scenarios with SUSY particles around the TeV scale, in which the region with very low $\tan\beta$ is simply ruled out by an excessively low prediction for the mass of the SM-like Higgs boson.

We finally mention that, in some instances, the ATLAS and CMS collaborations relied on a simplifying approach, the so-called "hMSSM" [66–69], to interpret their Higgs searches in the context of the MSSM. This approximation assumes that the Higgs sector is $\mathcal{CP}$ conserving, that all superparticles are too heavy to affect Higgs production and decays, that any non-decoupling SUSY corrections to the Higgs couplings are negligible, and that the radiative corrections to the elements other than (2, 2) in the mass matrix of the neutral $\mathcal{CP}$-even components of H_1 and H_2 are also negligible, i.e. $\Delta\mathcal{M}^2_{1j} \approx 0$ for $j = 1, 2$. In that case, the remaining radiative correction $\Delta\mathcal{M}^2_{22}$ can be expressed in terms of the parameters that determine the tree-level mass matrix (i.e. $\tan\beta$, M_Z and M_A) plus the smaller eigenvalue M_h, which is treated as an input and identified with the mass of the observed Higgs boson. Consequently, the larger eigenvalue M_H, the mixing angle α and the Higgs self-couplings can in turn be expressed in terms of just those four input parameters, of which only $\tan\beta$ and M_A are unknown. While the hMSSM approach brings some clear benefits – namely, the limited number of input parameters and the fact that the condition $M_h = 125.09$ GeV can be enforced all over the $(M_A, \tan\beta)$ plane – its predictions for the Higgs properties can be mapped only to regions of the MSSM parameter space in which the approximations of neglecting the $\Delta\mathcal{M}^2_{1j}$ corrections and the SUSY corrections to the Higgs couplings are justified. That, however, is not necessarily the case for small values of M_A and for rather large values of μ and $\tan\beta$. Moreover, near the lower-left corner of the $(M_A, \tan\beta)$ plane – i.e., for $\tan\beta \lesssim 1.5$ and $M_A \lesssim 200$ GeV – a lighter-scalar mass of about 125 GeV may require that the stops are as heavy as the GUT scale, putting into question the validity of the MSSM as the underlying high-energy theory [63]. In summary, an unambiguous interpretation of the results of the Higgs searches within the MSSM cannot really elude the dependence of the Higgs masses and couplings on the underlying SUSY parameters, and requires the definition of appropriate benchmark scenarios.

In this paper we propose six new benchmark scenarios for MSSM Higgs searches that are compatible with the most recent LHC results for the Higgs-boson properties and the bounds on masses and couplings of new particles. The first scenario is characterized by relatively heavy superparticles, so the Higgs phenomenology at the LHC resembles that of a 2HDM with MSSM-inspired Higgs couplings. The second and third scenario are characterized by some of the superparticles (staus and/or charginos and neutralinos) being lighter than the others and affecting the Higgs decays. The fourth and fifth scenario are characterized by the phenomenon of "alignment without decoupling" [11,12,70–73], in which one of the two neutral $\mathcal{CP}$-even Higgs scalars has SM-like couplings independently of the mass spectrum of the remaining Higgs bosons. Here, we present one scenario for each case, i.e. for either h or H being the SM-like scalar with mass around 125 GeV. Finally, the sixth scenario incorporates $\mathcal{CP}$ violation in the Higgs sector, giving rise to a strong admixture of the two heavier neutral states and leading to significant interference effects in their production and decay. We employ state-of-the-art calculations of the masses, branching ratios and production cross sections of the neutral Higgs bosons, including the effects of the resummation of large logarithmic corrections. In particular, we use `FeynHiggs` [20,24,28,32–34,41] to compute the masses, mixing and branching ratios of the neutral Higgs bosons, `SusHi` [74,75] to compute their production cross sections, and `HiggsBounds` [76–79] and `HiggsSignals` [80] to investigate the existing constraints on the parameter space of the scenarios.

The rest of the paper is organized as follows: in Sect. 2 we describe in detail the theoretical ingredients of our calculations; in Sect. 3 we define our six scenarios and discuss the bounds on their parameter space; finally, Sect. 4 contains our conclusions.

2 Theory setup

In this section we provide details on the precise predictions for the Higgs-boson masses, branching ratios and production cross sections that we use to define our new benchmark scenarios. Finally, we define the interference factors relevant to Higgs production and decay in the MSSM with $\mathcal{CP}$ violation.

2.1 Higgs-boson masses and branching ratios

For the calculation of the Higgs-boson masses we employ the latest version of FeynHiggs, 2.14.3. While the versions used to define the $\mathcal{CP}$-conserving scenarios of Ref. [15] and to produce the corresponding LHC-HXSWG files relied on a fixed-order (namely, full one-loop [33] and partial two-loop [34–38]) calculation of the masses, the latest version of the code includes also a full NLL and partial NNLL resummation of the corrections involving logarithms of the ratio between the SUSY scale and the EWSB scale [20,24,28]. Since our scenarios contain only moderately heavy superparticles, with masses up to about 2.5 TeV, we do not expect the inclusion of three- and higher-loop logarithmic terms to have a very large impact on the prediction for the SM-like Higgs mass. However, we stress that the full NLL resummation allows FeynHiggs to account – up to terms suppressed by inverse powers of the SUSY scale – also for the logarithmic part of the two-loop corrections involving the electroweak gauge couplings, which were not included in the original fixed-order calculation. As mentioned earlier, the combined effect of these refinements is a lower prediction (by 1 – 2 GeV) for the mass of the SM-like Higgs boson in our scenarios.

For the calculation of the Higgs masses and mixing in the MSSM with complex parameters, FeynHiggs includes the full one-loop results of Ref. [33] and the dominant two-loop corrections involving the top Yukawa coupling from Refs. [52–55]. Additional two-loop corrections involving the bottom Yukawa coupling, as well as the resummation of higher-order logarithmic effects, are approximated by interpolation of the corresponding corrections computed in the MSSM with real parameters.

The theoretical uncertainty of the prediction of FeynHiggs for the Higgs masses depends on the size and the origin of the radiative corrections, and should in principle be estimated separately at each point of the MSSM parameter space. For simplicity, in the definition of our scenarios we will stick to the global estimate of Refs. [41,42], and consider all points in the MSSM parameter space where FeynHiggs predicts the existence of a SM-like Higgs boson with a mass in the window 125.09 ± 3 GeV to be compatible with the Higgs-mass measurement at the LHC. This appears to be a conservative choice.

For future reference, we list here the values of the input flags of FeynHiggs 2.14.3 used in our predictions (see the online manual of the code [81] for more details):

$$\begin{aligned} \text{mssmpart} &= 4, & \text{higgsmix} &= 2, \\ \text{p2approx} &= 4, & \text{looplevel} &= 2, \\ \text{loglevel} &= 3, & \text{runningMT} &= 1, \\ \text{botResum} &= 1, & \text{tlCplxApprox} &= 0. \end{aligned}$$

In our fifth scenario (the one with a SM-like heavier scalar H) and in our sixth scenario (the one with $\mathcal{CP}$ violation) we use the charged-Higgs mass, $M_{H^\pm}$, rather than M_A as input parameter. In that case we set the input flags of FeynHiggs as above, with the exceptions of tlCplxApprox = 1 in the fifth scenario and higgsmix = 3, tlCplxApprox = 3 in the sixth scenario.

The branching ratios (BRs) for the decays of the neutral Higgs bosons are also computed with FeynHiggs.[1] The decays to quark and lepton pairs are evaluated at the full one-loop level, supplemented with UV-finite wave-function normalization factors (the "Z-factors") which ensure the correct on-shell properties of the external Higgs bosons [33,60,83–86], encoding the effect of scalar mixing at the same loop level as in the Higgs-mass calculation. The decays to bottom pairs also include a resummation of the $\tan\beta$-enhanced SUSY corrections [87–92], using one-loop formulae from Ref. [93] for the so-called "Δ_b terms". The decays to gluons or photons are computed at the lowest order (i.e., one loop), supplemented with the NLO-QCD contributions from diagrams involving gluons. For the decays to massive gauge bosons, FeynHiggs approximates the MSSM results by reweighting the SM results of the code Prophecy4F [94,95] with the appropriate Higgs–gauge-boson couplings. For the decays to Higgs bosons FeynHiggs implements a full one-loop calculation within the (complex) MSSM [85,86], improved with the resummation of potentially large logarithmic corrections. Finally, the decays to SUSY particles are computed at the tree level.

2.2 Production cross sections

The cross sections for Higgs-boson production via gluon fusion and bottom-quark annihilation are calculated with SusHi 1.7.0 [74,75] and with its extension to the MSSM with complex parameters, SusHiMi [58]. A link to FeynHiggs provides both the loop-corrected Higgs-boson masses and the matrix of Z-factors (the implementation of the latter in SusHi was discussed in Ref. [58]).

[1] It should be noted that in this work we do not strictly follow the prescription of the LHC-HXSWG for the calculation of the BRs [82]. However, the numerical differences are expected to be small, since they arise only from subdominant NLO corrections to some decay modes.

For both the top- and bottom-quark contributions to gluon fusion, SusHi includes the full next-to-leading order (NLO) results [96,97]. In addition, SusHi includes the next-to-NLO (NNLO) top-quark contributions in the heavy-quark effective theory [98–102] and even, for the SM-like scalar only, the next-to-NNLO (N^3LO) contributions, in a threshold expansion [103–105] which has been shown to closely match the exact result [106]. Compared with the results compiled by the LHC-HXSWG for the gluon-fusion cross section in the SM [19], SusHi omits only NNLO effects suppressed by powers of the top mass. In the MSSM with real parameters, scalar-quark (squark) and gluino contributions to gluon fusion are taken into account at NLO following Refs. [107–109], which rely on an expansion in inverse powers of the superparticle masses. In the MSSM with complex parameters these NLO contributions are interpolated, while the leading-order contribution incorporates the full phase dependence, see Ref. [58]. The $\tan\beta$-enhanced SUSY contributions to the Higgs–bottom-quark couplings are resummed using the Δ_b terms provided by FeynHiggs. The two-loop electroweak corrections to scalar production mediated by light quarks are included by reweighting the SM results of Refs. [110,111] with the appropriate Z-factors. The central renormalization and factorization scales are chosen to be $\mu_R = \mu_F = m_\phi/2$ (where ϕ is the produced Higgs boson). For the parton distribution functions (PDFs) we use the central set of PDF4LHC15_nlo_mc and PDF4LHC15_nnlo_mc [112] for the NLO and the NNLO/N^3LO contributions, respectively.

For Higgs-boson production in bottom-quark annihilation we employ the cross sections provided for the SM Higgs boson as a function of its mass by the LHC-HXSWG. Previously the LHC-HXSWG recommended "Santander-matched" cross sections [113], which combined results obtained in the five-flavor scheme [114] and in the four-flavor scheme [115–117]. In the definition of the new benchmark scenarios we follow the most recent recommendation [19], and use cross sections that consistently match between the two schemes and were obtained in the context of soft-collinear effective theory [118,119] (those coincide with the cross sections obtained in the so-called "fixed order plus next-to-leading log" (FONLL) approach [120,121]). However, we only take into account the part proportional to the bottom Yukawa coupling and omit the interference with the top-quark contribution. This is well justified in the regions where bottom-quark annihilation is experimentally relevant. The cross sections for the SM Higgs boson are reweighted with effective Higgs–bottom-quark couplings, using an effective mixing angle (or, in the case of $\mathcal{CP}$ violation, the matrix of Z-factors) in the scalar sector, and taking into account the resummation of $\tan\beta$-enhanced SUSY contributions as described earlier. In principle, the cross section for the production of a $\mathcal{CP}$-odd scalar in bottom-quark annihilation differs from the one of a $\mathcal{CP}$-even scalar, but this difference is negligible for $\mathcal{CP}$-odd-scalar masses beyond 100 GeV. Therefore, the SM cross section is also used to obtain a reweighted cross section for the $\mathcal{CP}$-odd scalar.

In our study we also take into account theoretical uncertainties for the gluon-fusion and bottom-quark-annihilation cross sections. For a thorough discussion of all potential sources of uncertainty for these two production channels in the MSSM we point the reader to Ref. [122]. Here, we follow a simplified approach: For the production of a $\mathcal{CP}$-even scalar via gluon fusion in the MSSM, the relative PDF+α_s uncertainties are assumed to coincide with those for the production of a SM Higgs boson of the same mass, which can be determined from the above-mentioned PDF4LHC15 sets (in particular, the largest deviation from the result obtained with the central PDF set is used as a symmetric relative uncertainty). For the production of a $\mathcal{CP}$-odd scalar via gluon fusion we generate a separate set of relative PDF+α_s uncertainties, assuming the field content of a 2HDM (in the scenario with $\mathcal{CP}$ violation, however, we apply the SM-inspired estimate to all three neutral scalars). The second source of uncertainty that we take into account for gluon fusion is the renormalization-scale dependence, which is estimated using the analytic approach described in Ref. [75]. For this purpose we take the minimal and maximal value of 100 equidistant scale choices between $\mu_R = m_\phi/4$ and $\mu_R = m_\phi$, and we use their difference as a symmetric uncertainty. The factorization-scale dependence, on the other hand, is known to be subdominant [122] and is not further considered. We finally add the renormalization-scale uncertainty and the PDF+α_s uncertainty in quadrature.

For bottom-quark annihilation we use the absolute uncertainties provided by the LHC-HXSWG for the SM Higgs boson, as a function of its mass and of the center-of-mass energy. Those include symmetric renormalization- and factorization-scale uncertainties, symmetric uncertainties related to the bottom-quark mass value and to the bottom-quark matching scale, and asymmetric PDF+α_s uncertainties. We add all downward (upward) shifts in quadrature, and transform the result into a total relative downward (upward) uncertainty. This relative uncertainty is applied to the production of all MSSM Higgs bosons, independently of the $\mathcal{CP}$ nature of the scalar under consideration.

The cross sections for Higgs production through vector-boson fusion, Higgsstrahlung and associated production with top quarks are computed with FeynHiggs, which reweights the SM predictions provided by the LHC-HXSWG with the appropriate MSSM/SM ratios of the couplings involved. Finally, the cross section for charged-Higgs production via $gg \to tbH^\pm$ and the corresponding uncertainty are read from a $(M_{H^\pm}, \tan\beta)$ grid for the type-II 2HDM provided by the LHC-HXSWG – relying on the calculations of Refs. [123–127] – and then reweighted with the

Δ_b corrections to the bottom Yukawa coupling provided by FeynHiggs.

2.3 Interference effects in Higgs production and decay

If two or more admixed Higgs bosons are nearly mass-degenerate and their Breit-Wigner propagators overlap, large interference effects occur in processes that involve these Higgs bosons in the s-channel. Rather than calculating the full process $I \to \sum_a h_a \to F$, involving the initial state I, the final state F and the exchange of all three of the Higgs mass eigenstates, in Refs. [59–61] an approximation was developed that combines the separate predictions for the production and decay of each mass eigenstate h_a with the respective interference contributions:

$$\sigma\left(I \to \sum_a h_a \to F\right) \simeq \sum_a \sigma(I \to h_a)\,(1+\eta_a^{IF})\,\mathrm{BR}(h_a \to F). \quad (1)$$

The calculation of the interference factors $\eta_a^{IF} \equiv \eta(I \to h_a \to F)$ is carried out at leading order only, however it takes into account the radiatively corrected Higgs masses, their total widths Γ_{h_a} and the Z-factors (the latter affect the internal Higgs-boson propagators). The advantage of this procedure is that higher-order corrections to the production and decay processes can be taken into account separately. This factorization is well justified if the total widths of the involved Higgs bosons are not too broad compared to the masses, and only neglects loop diagrams that connect initial and final states. For a more detailed explanation of this approximation we point the reader to Refs. [59–61].

In the so-called "decoupling limit" [70], realized in $\mathcal{CP}$-violating scenarios when $M_{H^\pm} \gg M_Z$, the lightest scalar h_1 hardly mixes with the two heavier scalars due to the large mass splitting, and thus remains almost purely $\mathcal{CP}$-even. In contrast, h_2 and h_3 become approximately mass-degenerate and can reach a sizable admixture, resulting in a large destructive interference effect in processes involving $h_{2,3}$ in the s-channel. The interference occurs as a consequence of the propagator structure that is also reflected in the Z-matrix, and is therefore a general feature of the decoupling limit in $\mathcal{CP}$-violating scenarios. Focusing on the h_2–h_3 interference, the interference factors are defined as

$$\eta_2^{IF} = \eta_3^{IF} \equiv \eta(I \to h_{2,3} \to F) = \frac{\sigma_{\mathrm{coh}}}{\sigma_{\mathrm{incoh}}} - 1, \quad (2)$$

where we distinguish the coherent cross section $\sigma_{\mathrm{coh}} = \sigma(|h_2 + h_3|^2)$ that sums up the amplitudes involving h_2 and h_3 from the incoherent cross section $\sigma_{\mathrm{incoh}} = \sigma(|h_2|^2) + \sigma(|h_3|^2)$. We implemented the calculation of the interference factors in SusHi for the initial states $I \in \{gg,\ b\bar{b}\}$ and the final states $F \in \{\tau\tau,\ b\bar{b},\ t\bar{t}\}$. The Higgs-boson propagators are numerically integrated for the invariant mass of the final state, m^F, within $m^F_{\mathrm{min,max}} = (m_{h_2} + m_{h_3})/2 \mp 5(\Gamma_{h_2} + \Gamma_{h_3})/2$, and SusHi provides the results in its output file for each combination of initial state, final state and intermediate Higgs boson. If such factors are eventually stored in the ROOT files of the LHC-HXSWG, they will be directly available to the experimental collaborations.

In the $\mathcal{CP}$-violating benchmark scenario that we will define in Sect. 3.7, by far the most relevant interference is obtained for the process $b\bar{b} \to h_{2,3} \to \tau^+\tau^-$, inducing a distortion of the exclusion bounds from searches of heavy Higgs bosons in the $\tau^+\tau^-$ final state with respect to the $\mathcal{CP}$-conserving case.

3 Definition of the benchmark scenarios

In this section we propose six new benchmark scenarios for MSSM Higgs searches at the LHC. All scenarios include a scalar with mass around 125 GeV and SM-like properties over large parts of the defined parameter space, and are compatible with recent searches for superparticles. In each scenario we leave two free parameters, such that searches for additional Higgs bosons can be presented in two-dimensional planes: one of the free parameters is always $\tan\beta$, while the other is either M_A (in the first four scenarios) or $M_{H^\pm}$ (in the last two). In all scenarios a significant region of the considered plane is still allowed by the searches for additional Higgs bosons at the LHC. In scans over the (M_A , $\tan\beta$) plane, $\tan\beta$ is varied between 0.5 and 60 and M_A between 70 GeV and 2 TeV, except in the fourth scenario where we focus on the region with $1 \le \tan\beta \le 20$ and 100 GeV $\le M_A \le 1$ TeV.

Indirect constraints on the MSSM parameter space such as those from requiring the correct Dark Matter density, from flavor observables or from the muon $g-2$, however interesting, depend to a large extent on parameters that are not crucial to Higgs-boson phenomenology. Following the spirit of previous benchmark proposals [13–15] we refrain from imposing additional constraints of this kind, with the obvious exception of the EDM constraints that are relevant to the definition of our scenario with $\mathcal{CP}$ violation, see Sect. 3.7.

3.1 SM input parameters

We follow the recommendation of the LHC-HXSWG in Ref. [19] and make use of the following SM input parameters:

$$\begin{aligned} &m_t^{\mathrm{pole}} = 172.5\ \mathrm{GeV}, \quad \alpha_s(M_Z) = 0.118, \\ &G_F = 1.16637 \times 10^{-5}\ \mathrm{GeV}^{-2}, \\ &m_b(m_b) = 4.18\ \mathrm{GeV}, \quad M_Z = 91.1876\ \mathrm{GeV}, \\ &M_W = 80.385\ \mathrm{GeV}. \end{aligned} \quad (3)$$

The dependence of the Higgs-boson properties on other quark and lepton masses is not very pronounced, and we stick to the default values of FeynHiggs. The value of the top-quark pole mass recommended by the LHC-HXSWG is below the current world average[2] of $173.21 \pm 0.51 \pm 0.71$ GeV [131]. We emphasize that, in our scenarios, a change of 0.7 GeV in the top-quark mass induces a variation of about 0.5–0.6 GeV in the MSSM prediction for the mass of the SM-like scalar. This significant parametric uncertainty should be kept in mind when considering whether a point in the MSSM parameter space is definitely ruled out by the Higgs-mass prediction. Indeed, a 2σ variation of the input value for top-quark mass could be accommodated by enlarging the interval of ± 3 GeV that we allow for M_h in view of the theoretical uncertainty of the MSSM prediction by a further ± 1.5 GeV.

3.2 SUSY input parameters

In principle, the definition of an MSSM scenario would require choices for about a hundred parameters in the soft-SUSY-breaking Lagrangian. However, since we are interested in the MSSM Higgs-boson phenomenology, in this study we focus on scenarios in which the soft-SUSY-breaking terms do not include new sources of flavor violation. Therefore, the precise values of the soft-SUSY-breaking mass and interaction terms for the first- and second-generation scalar fermions (sfermions) have only a limited effect on the predictions for the Higgs masses and mixing. We thus consider a common soft-SUSY-breaking mass $M_{\tilde{f}} = 2$ TeV for the first- and second-generation sfermions, compatible with the current exclusion bounds on squark masses by ATLAS [132,133] and CMS [134–136], and we set the corresponding Higgs–sfermion interaction terms A_f to zero. The remaining soft-SUSY-breaking parameters that define our different scenarios are: the third-generation squark mass parameters M_{Q_3}, M_{U_3} and M_{D_3}; the third-generation scalar-lepton (slepton) mass parameters M_{L_3} and M_{E_3}; the third-generation Higgs–sfermion interaction terms A_t, A_b and A_τ; the gaugino masses M_1, M_2 and M_3. In the first three of our scenarios we will not fix an input value for A_t, but rather for the combination $X_t = A_t - \mu \cot\beta$ which enters the left–right mixing term in the stop mass matrix and determines the correction to the mass of a SM-like scalar (we recall that μ is the Higgs/higgsino superpotential mass, which we treat as an additional input parameter). In the scenario where the heavier $\mathcal{CP}$-even scalar H is SM-like, several SUSY input parameters are defined as a function of the free parameter $M_{H^\pm}$, and thus vary over the considered $(M_{H^\pm}, \tan\beta)$ plane. We will consider all SUSY input parameters to be real, except in the scenario where we study $\mathcal{CP}$ violation, in which we introduce a non-zero phase for A_t.

The inclusion of radiative corrections in the predictions for the Higgs masses and production cross section requires that we specify a renormalization scheme for some of the SUSY input parameters. To be compatible with the two-loop calculations implemented in FeynHiggs and in SusHi (see Refs. [34–38,52–55,107–109], respectively, for the details) we will employ on-shell definitions for the parameters M_A, $M_{H^\pm}$, M_{Q_3}, M_{U_3}, M_{D_3}, A_t and A_b, whereas μ and $\tan\beta$ must be interpreted as $\overline{\text{DR}}$-renormalized parameters at a scale that FeynHiggs takes by default equal to the pole mass of the top quark.

3.3 Experimental constraints on the MSSM Higgs sector

The parameter space of our benchmark scenarios is already partially constrained by the limits obtained from the searches for additional Higgs bosons at the LHC, and by the requirement that one of the neutral scalars match the properties of the observed Higgs boson. We evaluate the former constraints with the code HiggsBounds [76–79], and the latter with the code HiggsSignals [80]. We stress, however, that the regions that are indicated in our plots below as disfavored by the properties of the observed Higgs boson and by the existing limits from Higgs searches are not meant to be regarded as "inaccessible", but should actually be explored in the experimental analyses. Our study of the existing constraints cannot truly replace a dedicated analysis of the proposed benchmark scenarios by ATLAS and CMS, which alone would be able to combine the results of different searches taking into account all correlations. In this section we briefly summarize the relevant features of the two codes used in our study.

3.3.1 Constraints from LHC searches for additional Higgs bosons

The code HiggsBounds tests each parameter point for 95% C.L. exclusion from Higgs searches at the LHC (as well as LEP and the Tevatron – however, those turn out to be irrelevant here). First, the code determines the most sensitive experimental search available – as judged by the expected limit – for each additional Higgs boson in the model. Then, only the selected channels are applied to the model, i.e. the predicted signal rate for the most sensitive search of each additional Higgs boson is compared to the observed upper limit, and in case the prediction exceeds the limit the parameter point is regarded as excluded. For more details on the procedure, we direct the reader to Ref. [79].

Among the searches for additional neutral Higgs bosons that are relevant in constraining our scenarios, the latest version, 5.2.0beta, of HiggsBounds includes: ATLAS [137] and CMS [138] searches for heavy Higgs

[2] Note, however, that the relation between the quoted world-average mass of the top quark and its pole mass is subject to debate, see e.g. Refs. [128–130].

bosons decaying to $\tau^+\tau^-$ pairs using about 36 fb^{-1} of Run-2 data, as well as the CMS results from Run 1 [139]; Run-1 and Run-2 searches by ATLAS [140,141] and CMS [142,143] for a heavy scalar decaying to a Z-boson pair; Run-1 searches by ATLAS [144] and Run-2 searches by CMS [145,146] for a heavy scalar decaying to a pair of 125-GeV scalars; Run-1 searches by ATLAS [147] and CMS [148] for the 125-GeV scalar decaying to a pair of lighter (pseudo)scalars; Run-1 searches by ATLAS [149] and CMS [150] for a heavy pseudoscalar decaying to a Z boson and the 125-GeV scalar. By comparing these results with the predictions of `SusHi` and `FeynHiggs` for production cross sections and decay branching ratios of the additional neutral Higgs bosons, `HiggsBounds` reconstructs the 95% C.L. exclusion contours in our scenarios. In the MSSM these constraints are typically stronger for large values of tan β, due to an enhancement of the production cross section of the heavier Higgs bosons in bottom-quark annihilation (in that case the most relevant searches are those for the decay to a $\tau^+\tau^-$ pair).

`HiggsBounds` also contains the available constraints from the searches for a charged Higgs boson by ATLAS and CMS. Most relevant in our scenarios are the constraints on the production of a light charged Higgs via a decaying top quark, $t \to H^+ b$, with subsequent decay $H^+ \to \tau^+\nu$ [151–154], as well as top-quark associated $H^\pm$ production, with subsequent decays to $\tau\nu$ [151–154] or tb [151,155,156] pairs.

In order to estimate the theoretical uncertainty in our determination of the excluded regions, we rely on the uncertainty estimates described in Sect. 2.2 for the gluon-fusion and bottom-quark annihilation cross sections. The most conservative (i.e., weakest) determination of the exclusion region is obtained by taking simultaneously the lowest values in the uncertainty range for both production processes of each of the heavier Higgs bosons, while the least conservative (i.e., strongest) determination is obtained by taking simultaneously the highest values in the uncertainty range.

3.3.2 *Constraints from the Higgs boson observed at the LHC*

We use the code `HiggsSignals` to test the compatibility of our scenarios with the observed Higgs signal, by comparing the predictions of `SusHi` and `FeynHiggs` for the signal strengths for Higgs production and decay – defined as $\mu^I \equiv \sigma^I/\sigma^I_{\rm SM}$ for each production process $I \to h$ and $\mu^F \equiv {\rm BR}^F/{\rm BR}^F_{\rm SM}$ for each decay $h \to F$ – against the measurements of the Higgs signal rates by ATLAS and CMS. The latest version, `2.2.0beta`, of `HiggsSignals` includes the combined ATLAS and CMS results from Run 1 of the LHC [4], as well as the available ATLAS [157–163] and CMS [164–173] results using about 36 fb^{-1} of Run-2 data. We determine the region of the parameter space compatible with these measurements by performing a log-likelihood ratio test within the two-dimensional MSSM scenario under consideration. In particular, we look for the "best-fit" point – i.e., the point yielding the minimum of the total χ^2 value of the signal strengths, $\chi^2_{\rm min}$ – over the full parameter plane, and then consider all points with $\Delta\chi^2 = \chi^2 - \chi^2_{\rm min} \leq 6.18$ to be allowed. This corresponds to a 2σ confidence level in the Gaussian limit. For reference, a SM Higgs boson with mass 125.09 GeV results in a total χ^2 value of $\chi^2_{\rm SM}/{\rm ndf} = 93.8/100$, where ndf is the number of degrees of freedom. The latter is given by the number of observables, which in our setup is $n_{\rm obs} = 100$, minus the number of model parameters, $n_{\rm par}$ (for the SM with fixed Higgs mass we have $n_{\rm par} = 0$, whereas for our two-dimensional MSSM planes we have $n_{\rm par} = 2$). We remark that, in the five of our scenarios in which the observed Higgs boson is identified with the lightest scalar, the best-fit point is located in the decoupling region where the additional Higgs bosons are all very heavy, and it provides essentially as good a fit to the measured Higgs rates as the SM. Even in the scenario where the observed Higgs boson is the heavier $\mathcal{CP}$-even scalar H, which is necessarily away from the decoupling region, the best-fit point is less than two units of χ^2 away from $\chi^2_{\rm SM}$.

A complication of our procedure is that, to account for the theoretical uncertainty of the mass calculation in `FeynHiggs`, we allow the prediction for the mass of the neutral scalar that we identify with the observed Higgs boson to lie in an interval of ± 3 GeV around the value measured at the LHC.[3] The predictions for cross sections and branching ratios show a non-negligible dependence on the Higgs-boson mass in this interval, potentially biasing the comparison with the LHC measurements. We will however assume that this mass dependence is approximately the same in the MSSM and in the SM, such that the predictions for the signal strengths are approximately independent of the Higgs mass in the allowed ± 3 GeV interval. Consequently, in each point of the parameter space the signal strengths computed by `SusHi` and `FeynHiggs` with the value of the Higgs-boson mass predicted by `FeynHiggs` can be compared directly to those obtained by ATLAS and CMS, in which the measured production and decay rates are normalized to the state-of-the-art SM predictions provided by the LHC-HXSWG [19] for the measured value of the Higgs-boson mass.

3.4 M_h^{125} scenario

In our first benchmark scenario, denoted as the "M_h^{125} scenario", all superparticles are chosen to be so heavy that pro-

[3] We recall that the theoretical uncertainty of the prediction for the Higgs mass arises from missing higher-order terms, and does not lend itself to a statistical interpretation. Therefore, we treat the ± 3 GeV interval as a hard cut, and we do not include the prediction for the Higgs mass in the determination of the χ^2 value.

duction and decays of the MSSM Higgs bosons are only mildly affected by their presence. In particular, the loop-induced SUSY contributions to the couplings of the lighter $\mathcal{CP}$-even scalar are small, and the heavy Higgs bosons with masses up to 2 TeV decay only to SM particles. Therefore, the phenomenology of this scenario at the LHC resembles that of a type-II 2HDM with MSSM-inspired Higgs couplings. The SUSY input parameters are fixed as

$$M_{Q_3} = M_{U_3} = M_{D_3} = 1.5\ \text{TeV}, \quad M_{L_3} = M_{E_3} = 2\ \text{TeV},$$
$$\mu{=}1\ \text{TeV}, \quad M_1{=}1\ \text{TeV}, \quad M_2{=}1\ \text{TeV}, \quad M_3 = 2.5\ \text{TeV},$$
$$X_t = 2.8\ \text{TeV}, \quad A_b = A_\tau = A_t. \tag{4}$$

The masses of the third-generation squarks and that of the gluino are safely above the current bounds from direct searches at the LHC (see Refs. [135,136,174–179] for the stops, Refs. [39,40,135,136,180,181] for the sbottoms and Refs. [132–136,180] for the gluino). To give an example, the stop pole masses are $m_{\tilde{t}_1} = 1340$ GeV and $m_{\tilde{t}_2} = 1662$ GeV, and for $\tan\beta = 20$ the sbottom pole masses are $m_{\tilde{b}_1} = 1480$ GeV and $m_{\tilde{b}_2} = 1521$ GeV. The value chosen for X_t is close to the one for which the maximal value of M_h is obtained. Due to the relatively large value of μ, chosen to ensure that the higgsinos are as heavy as the electroweak gauginos, the largest loop-induced SUSY effects arise through the resummation of the $\tan\beta$-enhanced corrections to the Higgs–bottom-quark couplings: the value of Δ_b is about 0.2 for $\tan\beta = 20$, and about 0.6 for $\tan\beta = 60$. We recall that in the decoupling limit, realized when $M_A \gg M_Z$, the effects of the Δ_b resummation cancel out for the couplings of the lighter $\mathcal{CP}$-even scalar, which becomes SM-like. However, such non-negligible values of Δ_b do affect the couplings to bottom pairs of the heavy Higgs bosons.

In Fig. 1 we present, in the $(M_A, \tan\beta)$ plane, the existing constraints on the M_h^{125} scenario from Higgs-boson searches at the LHC. The blue area represents the bounds from searches for heavy Higgs bosons (H or A) as determined by `HiggsBounds`, with the darker-blue band indicating the theoretical uncertainty of the exclusion. The green solid lines are the predictions of `FeynHiggs` for the mass of the lighter $\mathcal{CP}$-even scalar h: we see that in this scenario – for the top-mass value recommended by the LHC-HXSWG – M_h is always below 126 GeV. Finally, the hatched area is ruled out because the light scalar cannot be identified with the Higgs boson observed at the LHC: for low $\tan\beta$ the MSSM prediction for M_h falls outside the window 125.09 ± 3 GeV, and for low M_A the MSSM predictions for the production and decay rates of h are determined by `HiggsSignals` to be inconsistent with the LHC results. In particular, the almost vertical exclusion boundary at $M_A \approx 500{-}600$ GeV reflects the behavior of the $hb\bar{b}$ coupling, which determines the partial width for the dominant decay channel $h \to b\bar{b}$, and consequently affects the branching ratios for all the sub-

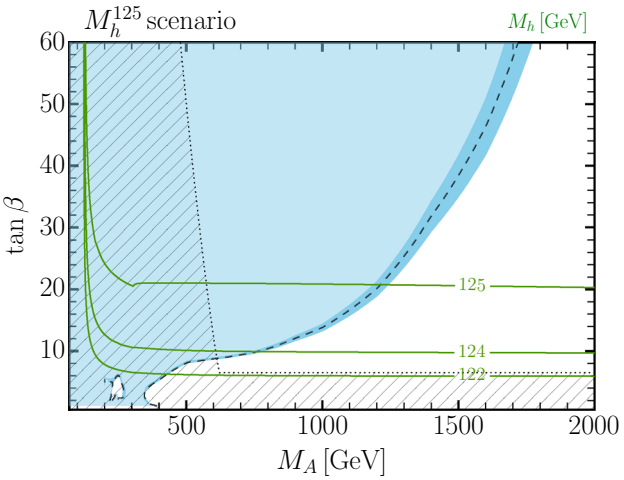

Fig. 1 Constraints on the M_h^{125} scenario from Higgs searches at the LHC, in the $(M_A, \tan\beta)$ plane. The green solid lines are predictions for the mass of the lighter $\mathcal{CP}$-even scalar h, the hatched area is excluded by a mismatch between the properties of h and those of the observed Higgs boson, and the blue area is excluded by the searches for additional Higgs bosons (the darker-blue band shows the theoretical uncertainty of the exclusion)

dominant decay channels. We recall that, at the tree level, the $hb\bar{b}$ coupling is rescaled with respect to its SM value by a factor of $-\sin\alpha/\cos\beta$, where α is the mixing angle that rotates the neutral-scalar components of H_1 and H_2 into the mass eigenstates h and H. For moderately large $\tan\beta$, the tree-level rescaling factor is well approximated by $1+2\,M_Z^2/M_A^2+\mathcal{O}(M_Z^4/M_A^4)$, i.e. it enhances the coupling at moderate M_A, then tends to the SM value in the decoupling limit of large M_A. The residual (mild) $\tan\beta$ dependence of the exclusion boundary at low M_A is due to the combined effects of the Δ_b corrections and of $\tan\beta$-enhanced stop-loop contributions to the Higgs mixing, see Ref. [73], which in this scenario suppress the $hb\bar{b}$ coupling at large $\tan\beta$.

Figure 1 shows that a significant region of the $(M_A, \tan\beta)$ plane of the M_h^{125} scenario is still allowed by the LHC results from Higgs searches: it starts at $M_A \approx 600$ GeV and $\tan\beta \approx 6{-}8$, and it opens up to higher values of $\tan\beta$ for increasing M_A. The constraints at high values of $\tan\beta$ arise essentially from the searches for $H/A \to \tau^+\tau^-$ at the LHC with 13 TeV center-of-mass energy [137,138]. On the other hand, values of $\tan\beta$ lower than about 6 are ruled out in the M_h^{125} scenario by the prediction of a mass below 122.09 GeV for the SM-like scalar. The hole in the blue area around $M_A \approx 250$ GeV and $\tan\beta \approx 4$ corresponds to a region of the parameter space where H has significant branching fractions to ZZ and hh pairs, but no individual search is strong enough to yield an exclusion. However, this region is ruled out by the requirement that the properties of h match those of the observed Higgs boson.

3.5 Scenarios with light superparticles

Light superparticles, in particular charginos and neutralinos – which we collectively denote as electroweak (EW)-inos – and third-generation sfermions, can substantially influence the Higgs phenomenology, see e.g. Refs. [15,182–187]. This may happen through loop contributions to the Higgs boson couplings to SM particles, as well as, when kinematically possible, through direct decays of the Higgs bosons into superparticles.

Reference [15] proposed a scenario with degenerate soft-SUSY-breaking parameters $M_{Q_3} = M_{U_3} = 500$ GeV and stop mixing $X_t = 1$ TeV, resulting in lighter and heavier stop masses of about 325 GeV and 670 GeV, respectively. The parameters M_1, M_2 and μ were chosen in such a way that the lighter stop decays almost entirely to the lightest neutralino and a charm quark, thus evading the Run-1 searches for stops at the LHC. However, as mentioned in Sect. 1, such "light-stop" scenarios are now strongly constrained by monojet searches by ATLAS [39] and CMS [40]. Moreover, in the light-stop scenario of Ref. [15] the recent refinements in the Higgs-mass calculation of `FeynHiggs` result in a prediction for M_h that undershoots the observed value by more than 3 GeV. Even if it was possible to evade the Run-2 stop searches by further tuning the EW-ino masses, a scenario with a lighter-stop mass of about 300 – 400 GeV would require a large splitting between M_{Q_3} and M_{U_3} in order to raise the prediction for M_h through radiative corrections involving the heavier stop. However, in that case the accurate resummation of large logarithmic effects would require a specific EFT setup – not yet implemented in `FeynHiggs` or in any other public code – in which some of the squark masses are close to the EW scale while others are in the multi-TeV region, see e.g. Refs. [188,189]. Moreover, the results of Refs. [107–109], used by `SusHi` to compute the two-loop SUSY contributions to the gluon-fusion cross section, rely on a heavy-SUSY expansion valid only when the mass of the produced Higgs boson is less than twice the lighter-stop mass, leading to an upper bound on the values of M_A allowed in our analysis. In view of these limitations in the codes, and of the tuning of the MSSM parameters that would be required to evade the bounds from squark searches at the LHC, we refrain from proposing a new "light-stop" scenario for the time being.

In contrast, the bounds on light non-colored superparticles are still weak, and can bring in phenomenologically interesting aspects. For certain observables, e.g. the muon $g-2$, the contributions of non-colored states can significantly reduce the tension between the SM prediction and experimental measurements, see e.g. Refs. [11,190]. For what concerns Higgs phenomenology, the rate of the loop-induced decay of the lighter $\mathcal{CP}$-even scalar to two photons can be significantly altered by the contributions of light staus or light charginos. In particular, the former are enhanced for large values of $\mu \tan\beta$, while the latter are enhanced for low values of $\tan\beta$ through the wino–higgsino mixing. In addition, the decay of the lighter $\mathcal{CP}$-even scalar to bino-like neutralinos can be relevant if the latter are sufficiently light. For the heavy Higgs bosons, the decays to the light superparticles open up, and they accordingly reduce the branching ratios into SM particles.

In this paper we introduce two scenarios with light superparticles: one with light staus and light EW gauginos, and another in which all of the sfermions are heavy but all of the EW-inos (i.e., both gauginos and higgsinos) are light. They can be viewed as an update of the light-SUSY scenarios previously introduced in Ref. [15].

3.5.1 $M_h^{125}(\tilde{\tau})$ scenario

In this scenario the SUSY input parameters are fixed as

$$\begin{aligned} &M_{Q_3} = M_{U_3} = M_{D_3} = 1.5\ \text{TeV}, \quad M_{L_3} = M_{E_3} = 350\ \text{GeV}, \\ &\mu = 1\ \text{TeV}, \quad M_1 = 180\ \text{GeV}, \quad M_2 = 300\ \text{GeV}, \\ &M_3 = 2.5\ \text{TeV}, \quad X_t = 2.8\ \text{TeV}, \quad A_b = A_t, \\ &A_\tau = 800\ \text{GeV}. \end{aligned} \tag{5}$$

The parameters that determine the stop, sbottom and gluino masses are the same as in the M_h^{125} scenario, see Eq. (4), but the soft-SUSY-breaking masses and trilinear interaction term for the staus are considerably reduced. The left–right mixing term in the stau mass matrix is $m_\tau X_\tau$, where $X_\tau = A_\tau - \mu \tan\beta$, thus the splitting between the two stau mass eigenvalues increases with $\tan\beta$. The EW-gaugino masses M_1 and M_2 are in turn reduced with respect to their values in the M_h^{125} scenario. Due to the hierarchy among the parameters M_1, M_2 and μ, the EW-ino spectrum is essentially not mixed: the lightest neutralino is mostly bino with mass around 180 GeV, the lighter chargino and the second-lightest neutralino are mostly winos with masses around 300 GeV, and the heavier EW-inos are mostly higgsinos with masses around 1 TeV. Our choices of parameters in the stau and EW-ino sectors ensure that the lightest SUSY particle (LSP) is the lightest neutralino, except for the region with $\tan\beta \gtrsim 52$ where the large value of X_τ causes the lighter stau $\tilde{\tau}_1$ to become the LSP. However, as we discuss below, such high values of $\tan\beta$ are almost entirely excluded by other constraints.

The combined lower bounds on the lighter-stau and lighter-chargino masses from the LEP experiments are $m_{\tilde{\tau}_1} \gtrsim 90\,\text{GeV}$ [191] and $m_{\tilde{\chi}_1^\pm} > 103.5\,\text{GeV}$ [192], respectively, i.e. well below the values that characterize the $M_h^{125}(\tilde{\tau})$ scenario. At the Run 2 of the LHC, searches for direct stau-pair production are not yet sensitive enough to constrain this scenario [193]. For what concerns the EW-inos, the most

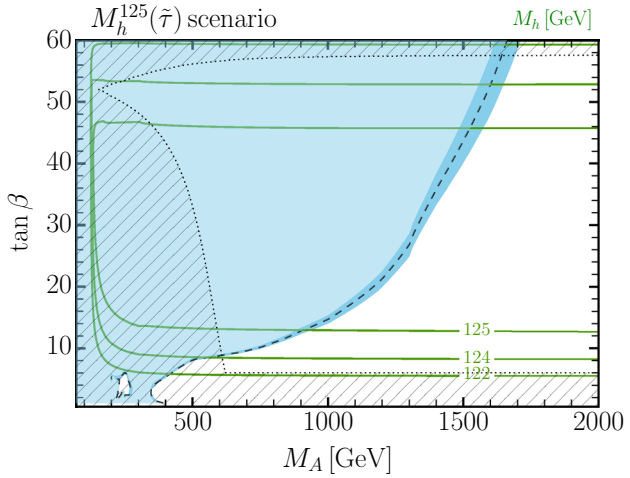

Fig. 2 Constraints on the $M_h^{125}(\tilde{\tau})$ scenario from Higgs searches at the LHC, in the (M_A , tan β) plane. The green solid lines are predictions for the mass of the lighter $\mathcal{CP}$-even scalar h, the hatched area is excluded by a mismatch between the properties of h and those of the observed Higgs boson, and the blue area is excluded by the searches for additional Higgs bosons (the darker-blue band shows the theoretical uncertainty of the exclusion)

relevant channels at the LHC are $\tilde{\chi}_1^+ \tilde{\chi}_1^-$ and $\tilde{\chi}_1^\pm \tilde{\chi}_2^0$ pair production. The reach of these searches in the $M_h^{125}(\tilde{\tau})$ scenario depends on the dominant decay mechanism of the wino-like EW-inos. For tan $\beta \gtrsim 20$ the mass of the lighter stau is less than 300 GeV, and the wino-like EW-inos decay to the lightest, bino-like neutralino mostly via an intermediate on-shell stau, resulting in final states with tau leptons and missing energy. In contrast, for lower values of tan β the lighter stau is heavier than 300 GeV, and the dominant decays of the wino-like EW-inos are to the lightest neutralino plus a gauge boson (or, when allowed, a Higgs boson – see Ref. [194]), in which case the most sensitive searches are for final states with light leptons (electrons or muons) and missing energy. We checked that the current results of the LHC searches for EW-ino pair production, both with [193,195] and without [196–198] tau leptons in the final state, cannot exclude an MSSM scenario with bino mass around 180 GeV and wino mass around 300 GeV. An eventual tightening of the bounds from LHC searches could be compensated for by raising the value of M_1, at the price of lowering the value of tan β for which the lighter stau becomes the LSP.

In Fig. 2 we present, in the (M_A , tan β) plane, the existing constraints on the $M_h^{125}(\tilde{\tau})$ scenario from Higgs-boson searches at the LHC. The meaning of the different curves is the same as in Fig. 1. The blue region excluded by the LHC searches for heavy Higgs bosons shows only a mild variation with respect to the M_h^{125} scenario of Fig. 1, namely a small change in the slope of the exclusion boundary around $M_A \approx 1.3$ TeV. On the other hand, significant changes are visible in the hatched region excluded by the properties of the lighter $\mathcal{CP}$-even scalar h. For moderate values of tan β, where the corrections to the Higgs mass matrix that involve staus are not important, the predictions of `FeynHiggs` for the mass of the lighter $\mathcal{CP}$-even scalar (see the dashed lines) show a mild increase with respect to the M_h^{125} scenario, which can be traced back to the lower values adopted for M_1 and M_2 in the $M_h^{125}(\tilde{\tau})$ scenario. Nevertheless, the prediction for M_h remains below 126 GeV all over the (M_A , tan β) plane, and the lowest value of tan β allowed by the ± 3 GeV theoretical uncertainty is about 6. In addition, for very large values of tan β the corrections involving staus cause the predictions for M_h to decrease, reaching the lowest allowed value of $M_h = 122.09$ GeV for tan $\beta \approx 60$. However, the hatched region in Fig. 2 shows that the requirement that the production and decay rates of the lighter $\mathcal{CP}$-even scalar be SM-like rules out values of tan β larger than about 58. This is in contrast with the M_h^{125} scenario, see Fig. 1, where at large tan β the lighter $\mathcal{CP}$-even scalar is sufficiently SM-like as long as $M_A \gtrsim 500$ GeV. Finally, we remark that the region with tan $\beta \gtrsim 52$, in which the lighter stau would be the LSP, is largely ruled out by the combination of the blue and hatched regions.

In order to understand the shape of the exclusion regions in Fig. 2, we now investigate how the presence of light superparticles affects the decays of the MSSM Higgs bosons in the $M_h^{125}(\tilde{\tau})$ scenario. As discussed, e.g., in Ref. [184], both light-chargino and light-stau contributions can affect the amplitude for the loop-induced decay of the lighter $\mathcal{CP}$-even scalar to two photons, $h \to \gamma\gamma$. However, the chargino contributions scale like $1/\tan\beta$, and are therefore suppressed for the moderate-to-large values of tan β required to obtain $M_h \geq 122.09$ GeV. In contrast, the stau contributions contain a term scaling like $\tan^2\beta$, and can therefore become relevant when tan β is sufficiently large. The green solid lines in the left plot of Fig. 3 show, in the (M_A , tan β) plane, the decay width $\Gamma(h \to \gamma\gamma)$ as computed by `FeynHiggs` in the $M_h^{125}(\tilde{\tau})$ scenario, normalized to the corresponding width of a SM Higgs boson of the same mass. To guide the eye, the boundaries of the blue and the hatched exclusion regions of Fig. 2 are also shown as a dashed and a dotted black line, respectively. We see that the EW-ino contributions can exceed 1% only in a low-tan β region that is already excluded by the properties of the SM-like Higgs boson, as indicated by the dotted line, whereas the stau contributions can increase the diphoton width of the lighter $\mathcal{CP}$-even scalar by more than 10% when tan $\beta \gtrsim 50$.

The right plot in Fig. 3 shows instead the branching ratio for $h \to \gamma\gamma$, again normalized to the corresponding quantity in the SM. We see that also the branching ratio can become significantly enhanced at large tan β – resulting in the excluded strip on the top margin of Fig. 2 – but the curves of constant MSSM/SM ratio show a markedly different behavior from those in the left plot: indeed, when tan $\beta < 50$ the

branching ratio can also be *suppressed* by more than 10%, for values of M_A extending up to about 500 GeV. This is mainly due to the behavior of the $hb\bar{b}$ coupling, which – as described in Sect. 3.4 – is enhanced at low M_A, thus suppressing the branching ratios for all subdominant decay channels such as $h \to \gamma\gamma$, and then relaxes to its SM value when M_A is large enough.

For very large $\tan\beta$, the corrections to the Higgs mixing angle due to stau loops can also have a significant impact on the $hb\bar{b}$ coupling in the $M_h^{125}(\tilde{\tau})$ scenario. In particular, for $\tan\beta \approx 52$ the scenario manifests the so-called "alignment without decoupling" (see Sect. 3.6 below), where the $hb\bar{b}$ coupling remains SM-like for all values of M_A, so the variation in the branching ratio for $h \to \gamma\gamma$ just follows from the variation in the corresponding width. We note, however, that for such large value of $\tan\beta$ the LHC searches for $H/A \to \tau^+\tau^-$ already rule out the region with $M_A \lesssim 1.6$ TeV, see Fig. 2.

When kinematically allowed, the decays of the heavier $\mathcal{CP}$-even scalar H and of the $\mathcal{CP}$-odd scalar A to light superparticles reduce the branching ratios of their decays to tau pairs, potentially weakening the exclusion bounds from the LHC searches. The left plot in Fig. 4 shows, in the $(M_A\,, \tan\beta)$ plane, the total branching ratio for the decays of H to stau pairs, whereas the right plot shows the total branching ratio for the decays of H to chargino or neutralino pairs.

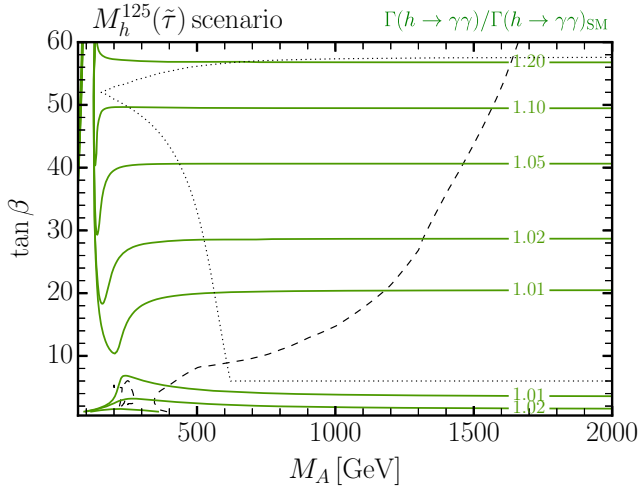

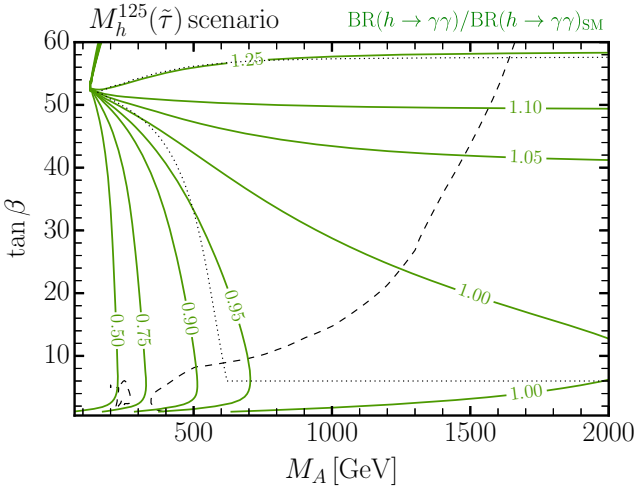

Fig. 3 Left: Decay width of the lighter $\mathcal{CP}$-even scalar into photons as a function of M_A and $\tan\beta$ in the $M_h^{125}(\tilde{\tau})$ scenario, normalized to the corresponding width of a SM Higgs boson of the same mass. Right: same as the left plot for the branching ratio of the decay $h \to \gamma\gamma$. In each plot, the boundaries of the blue and the hatched exclusion regions of Fig. 2 are also shown as a dashed and a dotted black line, respectively

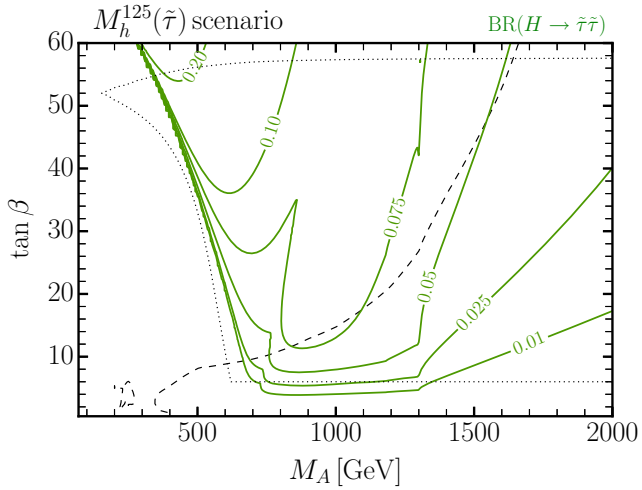

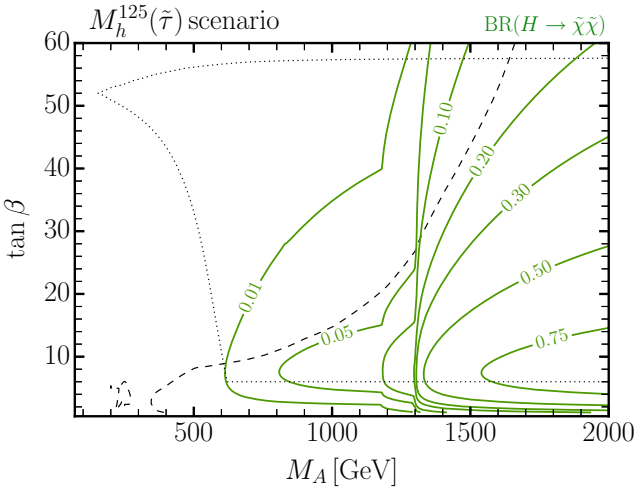

Fig. 4 Left: Total branching ratio for the decays of the heavier $\mathcal{CP}$-even scalar H into stau pairs, as a function of M_A and $\tan\beta$ in the $M_h^{125}(\tilde{\tau})$ scenario. Right: same as the left plot for the total branching ratio of the decays of H into chargino or neutralino pairs. In each plot, the boundaries of the blue and the hatched exclusion regions of Fig. 2 are also shown as a dashed and a dotted black line, respectively

In both cases a sum is taken over all the kinematically allowed combinations of particles in the final state. The plots show that the decays of H to stau pairs can be most relevant, with a branching ratio above 20%, in a region with relatively small M_A and large $\tan\beta$ that is already well excluded by the LHC searches for $H/A \to \tau^+\tau^-$. On the other hand, the decays of H to EW-inos can be most relevant for $M_A \gtrsim 1.3$ TeV, when the final states involving a higgsino-like EW-ino and a wino-like EW-ino are kinematically open. This explains the mild change in the slope of the black dashed line (i.e., the boundary of the region excluded by `HiggsBounds`) around that value of M_A. The right plot of Fig. 4 also shows that the total branching ratio for the decays of H to EW-inos is maximized, and can exceed 75%, in the "intermediate" region around $\tan\beta \approx 7$, where the decays of the heavy Higgs bosons to $t\bar{t}$ pairs are still suppressed and those to $b\bar{b}$ and $\tau^+\tau^-$ pairs are only weakly enhanced. We remark that the decays of the $\mathcal{CP}$-odd scalar to EW-ino pairs follow a similar pattern as the corresponding decays of the heavier $\mathcal{CP}$-even scalar. However, for the decays of the $\mathcal{CP}$-odd scalar to staus only the channel $A \to \tilde{\tau}_1\tilde{\tau}_2$ is open at tree level, resulting in a maximal branching ratio of about 14% in the (already excluded) region with $M_A \approx 800$ GeV and large $\tan\beta$.

Finally, it has long been known that charge- and color-breaking (CCB) minima of the scalar potential can arise in the presence of large left–right sfermion mixing [199–204]. In particular, vacuum stability bounds on the parameters that affect the stau masses have been recently discussed in Refs. [205–207]. The requirement that the lifetime of the ordinary EW-breaking minimum be longer than the age of the Universe constrains the combination $\tan\beta/(1+\Delta_\tau)$, where Δ_τ represents non-decoupling, $\tan\beta$-enhanced SUSY corrections to the relation between the tau mass and Yukawa coupling (they are analogous to the Δ_b effects in the bottom/sbottom sector, but generally smaller as they involve only the EW gauge couplings). For example, with the choices of SUSY parameters given in Eq. (5) the approximate bounds presented in Refs. [205,207] are violated when $\tan\beta/(1+\Delta_\tau) \gtrsim 50$. However, as discussed in Ref. [206], the vacuum stability bounds may also depend non-trivially on the combination $A_\tau/(1+\Delta_\tau)$, as well as on the $\mathcal{CP}$-odd scalar mass M_A. We have therefore used the code `Vevacious` [208–211] to check numerically the stability of the ordinary EW-breaking minimum in the $M_h^{125}(\tilde{\tau})$ scenario all over the $(M_A, \tan\beta)$ plane, neglecting loop corrections to the potential and thermal effects. We found that the ordinary EW-breaking minimum can be unstable only in a narrow region at large $\tan\beta$ which is already mostly excluded by the LHC searches. In a larger part of the parameter space one or more deeper minima with non-zero stau vevs exist, but the tunneling time from the ordinary minimum to charge-breaking minima exceeds the lifetime of the Universe.

3.5.2 $M_h^{125}(\tilde{\chi})$ scenario

In this scenario the SUSY input parameters are fixed as

$$\begin{aligned} &M_{Q_3} = M_{U_3} = M_{D_3} = 1.5\ \text{TeV}, \quad M_{L_3} = M_{E_3} = 2\ \text{TeV}, \\ &\mu = 180\ \text{GeV}, \quad M_1 = 160\ \text{GeV}, \quad M_2 = 180\ \text{GeV}, \\ &M_3 = 2.5\ \text{TeV}, \quad X_t = 2.5\ \text{TeV}, \quad A_b = A_\tau = A_t\,. \end{aligned} \tag{6}$$

The parameters M_1, M_2 and μ have relatively small values that are all close to each other, giving rise to a significant mixing between higgsinos and gauginos and a compressed EW-ino mass spectrum. In particular, the mass of the lightest neutralino $\tilde{\chi}_1^0$ varies between 105 GeV for $\tan\beta = 5$ and 118 GeV for the largest considered values of $\tan\beta$, the mass of the lighter chargino $\tilde{\chi}_1^\pm$ varies between 119 GeV and 131 GeV in the same range of $\tan\beta$, and the mass of the second-lightest neutralino $\tilde{\chi}_2^0$ is about 165 GeV independently of $\tan\beta$. The soft-SUSY-breaking masses for the gluino and for the sfermions are the same as in the M_h^{125} scenario, but the stop mixing parameter X_t is slightly reduced, to partially compensate for an enhancement in the prediction of the SM-like Higgs mass due to light EW-inos. The sbottom mixing parameter $X_b = A_b - \mu\tan\beta$ is instead significantly lowered by the small value of μ.

Compressed EW-ino mass spectra are probed at the LHC by searches for events with soft leptons and missing transverse momentum in the final state [212,213]. In scenarios where the slepton-mediated decays of the EW-inos are suppressed by large slepton masses, the most sensitive channel is the production of a $\tilde{\chi}_1^\pm\,\tilde{\chi}_2^0$ pair, followed by the decay of each EW-ino into a virtual gauge boson – which in turn decays to leptons – plus the lightest neutralino. However, the interpretation of the LHC searches for EW-inos in this channel leads to the strongest bounds when $\tilde{\chi}_1^\pm$ and $\tilde{\chi}_2^0$ are assumed to be mass-degenerate pure winos. A full recast of those searches to the $M_h^{125}(\tilde{\chi})$ scenario – in which $\tilde{\chi}_1^\pm$ is a mixture of wino and higgsino and $\tilde{\chi}_2^0$ is mostly bino and somewhat heavier – is beyond the scope of our paper and best left to the experimental collaborations, but we did perform a naive study with `CheckMATE` [214–220], using `SDecay` [221] to compute the decays of the EW-inos. We found that the $M_h^{125}(\tilde{\chi})$ scenario is not constrained by the CMS and ATLAS searches of Refs. [212,213], which were based on 36 fb^{-1} of Run-2 data.[4] Some constraints appear to arise from a multilepton search by CMS [223], but only at low values of $\tan\beta$ that are mostly ruled out by the prediction for M_h.

In Fig. 5 we present, in the $(M_A, \tan\beta)$ plane, the existing constraints on the $M_h^{125}(\tilde{\chi})$ scenario from Higgs-boson searches at the LHC. The meaning of the different curves is

[4] Curiously, `CheckMATE` does find constraints on the $M_h^{125}(\tilde{\chi})$ scenario arising from the search presented in a preliminary CMS note, Ref. [222], which was based only on 13 fb^{-1} of data. We could not find a convincing explanation for this apparent inconsistency.

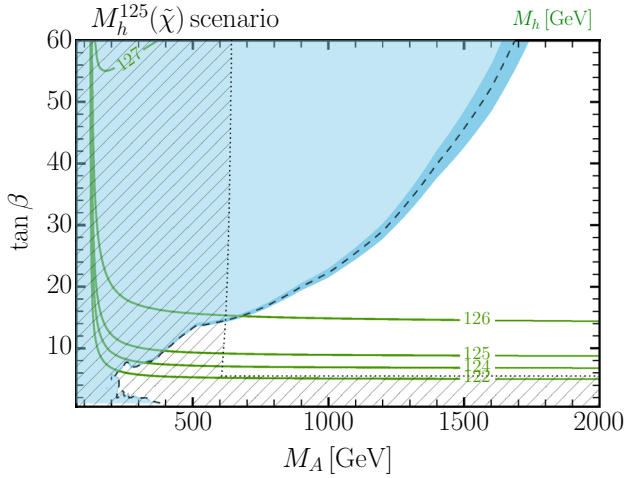

Fig. 5 Constraints on the $M_h^{125}(\tilde{\chi})$ scenario from Higgs searches at the LHC, in the $(M_A\,,\tan\beta)$ plane. The green solid lines are predictions for the mass of the lighter $\mathcal{CP}$-even scalar h, the hatched area is excluded by a mismatch between the properties of h and those of the observed Higgs boson, and the blue area is excluded by the searches for additional Higgs bosons (the darker-blue band shows the theoretical uncertainty of the exclusion)

the same as in Fig. 1. In the lower-left corner of the plane, the blue region that is excluded by the LHC searches for additional Higgs bosons is significantly modified compared to the corresponding regions in the M_h^{125} and $M_h^{125}(\tilde{\tau})$ scenarios, see Figs. 1 and 2. This feature will be further discussed below. Concerning the hatched region excluded by the properties of the lighter $\mathcal{CP}$-even scalar h, the reduced $\tan\beta$ dependence (with respect to Figs. 1 and 2) in the boundary around $M_A \approx 600$ GeV is due to the small value of μ, which suppresses the $\tan\beta$-enhanced corrections to the $hb\bar{b}$ coupling. Despite the reduction in X_t, the predictions for the mass of the lighter $\mathcal{CP}$-even scalar show a mild increase with respect to the M_h^{125} scenario. However, they remain below 127 GeV, except in the upper-left corner of the $(M_A\,,\tan\beta)$ plane. The lowest value of $\tan\beta$ allowed by the ± 3 GeV theoretical uncertainty in M_h is about 5.

We now discuss the effect of the presence of light EW-inos on the decays of the MSSM Higgs bosons. The left plot in Fig. 6 shows, in the $(M_A\,,\tan\beta)$ plane, the decay width of the lighter $\mathcal{CP}$-even scalar to two photons in the $M_h^{125}(\tilde{\chi})$ scenario, normalized to the corresponding width of a SM Higgs boson of the same mass. As in the case of the $M_h^{125}(\tilde{\tau})$ scenario, see the left plot in Fig. 3, the EW-ino contributions are most relevant at low values of $\tan\beta$. However, the small value of the higgsino mass parameter μ ensures that in the $M_h^{125}(\tilde{\chi})$ scenario the effect on the prediction for $\Gamma(h \to \gamma\gamma)$ is much stronger, increasing it by about 10% for $\tan\beta \approx 4$. Again, this effect must compete with the variation in the width for the dominant decay channel $h \to b\bar{b}$, which is enhanced at low M_A and relaxes to its SM value at large M_A. This is illustrated by the right plot in Fig. 6, which shows the branching ratio for the decay $h \to \gamma\gamma$ in the $M_h^{125}(\tilde{\chi})$ scenario normalized to the corresponding quantity in the SM. In addition to the enhancement of the EW-ino effects, which can exceed 5% in a sliver of the allowed region at low $\tan\beta$ and large M_A, the absence of stau-induced effects at large $\tan\beta$ explains the differences with the analogous plot for the $M_h^{125}(\tilde{\tau})$ scenario, see Fig. 3.

Figure 7 shows, in the $(M_A\,,\tan\beta)$ plane, the branching ratio for the decays of the heavier $\mathcal{CP}$-even scalar H (left plot) or the $\mathcal{CP}$-odd scalar A (right plot) to chargino or neutralino pairs in the $M_h^{125}(\tilde{\chi})$ scenario. A sum is taken over all the

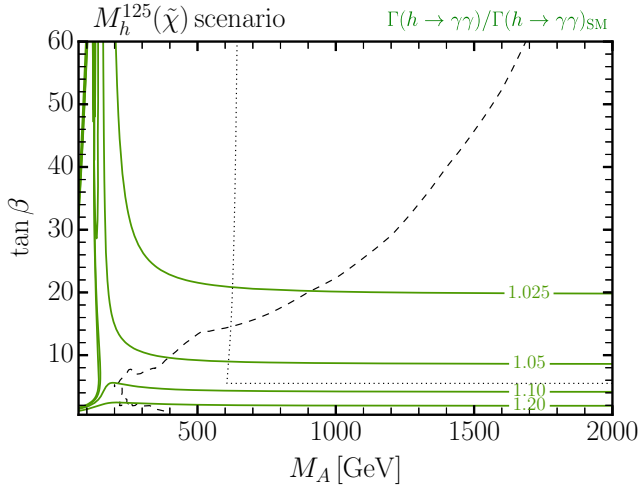

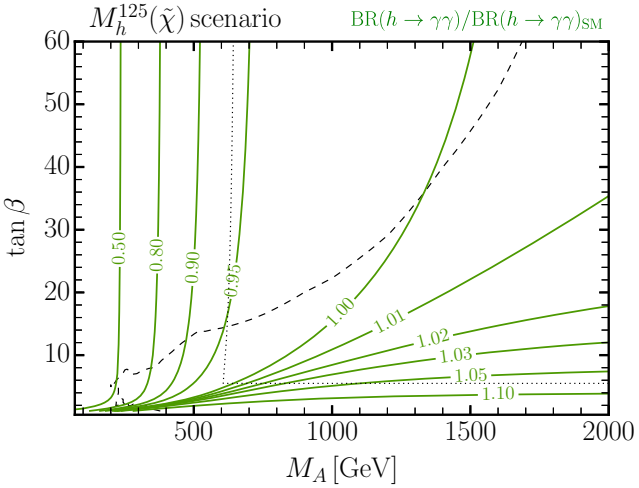

Fig. 6 Left: Decay width of the lighter $\mathcal{CP}$-even scalar into photons as a function of M_A and $\tan\beta$ in the $M_h^{125}(\tilde{\chi})$ scenario, normalized to the corresponding width of a SM Higgs boson of the same mass. Right: same as the left plot for the branching ratio of the decay $h \to \gamma\gamma$. In each plot, the boundaries of the blue and the hatched exclusion regions of Fig. 5 are also shown as a dashed and a dotted black line, respectively

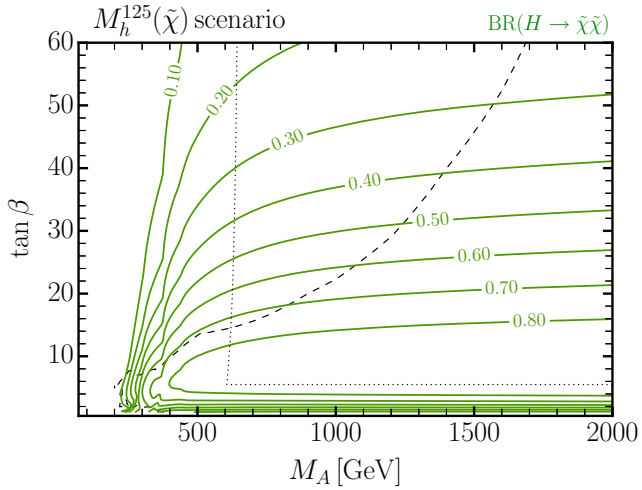

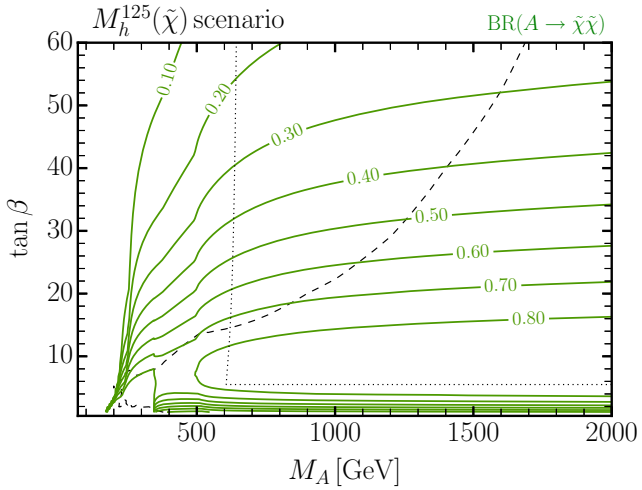

Fig. 7 Branching ratio for the decays of the heavier $\mathcal{CP}$-even scalar H (left) or the $\mathcal{CP}$-odd scalar A (right) into EW-ino pairs, as a function of M_A and $\tan\beta$ in the $M_h^{125}(\tilde{\chi})$ scenario. A sum is taken over all the kinematically allowed combinations of particles in the final state. In each plot, the boundaries of the blue and the hatched exclusion regions of Fig. 5 are also shown as a dashed and a dotted black line, respectively

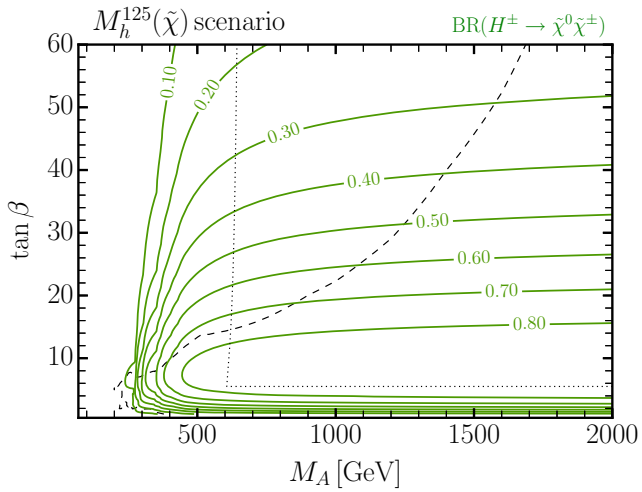

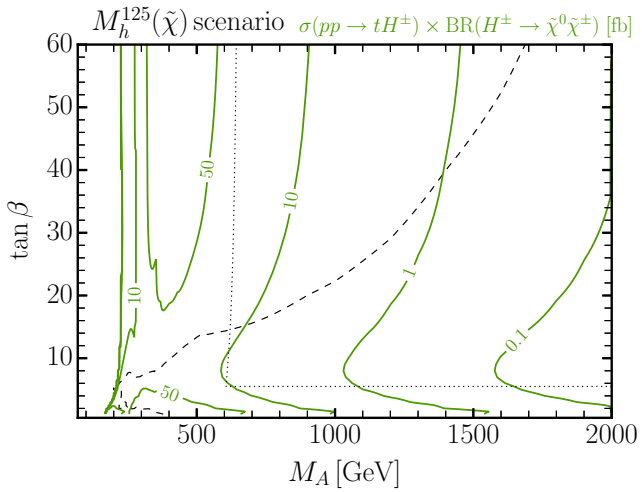

Fig. 8 Left: Branching ratio for the charged-Higgs decays to chargino–neutralino pairs, as a function of M_A and $\tan\beta$ in the $M_h^{125}(\tilde{\chi})$ scenario. A sum is taken over all the kinematically allowed combinations of particles in the final state. Right: Total rate (in fb) for the production of a charged Higgs boson in association with a top quark, followed by its decay to EW-inos, at the LHC with 13 TeV center-of-mass energy. In each plot, the boundaries of the blue and the hatched exclusion regions of Fig. 5 are shown as a dashed and a dotted black line, respectively

kinematically allowed combinations of particles in the final state, and the dents visible in the curves for $M_A \lesssim 500$ GeV mark the corresponding thresholds (as well as, at low $\tan\beta$, the threshold for the $t\bar{t}$ channel). The relatively low value of the higgsino mass parameter μ in the $M_h^{125}(\tilde{\chi})$ scenario ensures that the decays to one higgsino-like EW-ino and one wino-like EW-ino open up at much lower values of M_A than in the $M_h^{125}(\tilde{\tau})$ scenario. Indeed, for $5 \lesssim \tan\beta \lesssim 10$ the branching ratios for the decays of the heavy Higgs bosons to EW-inos can exceed 80% already for $M_A \gtrsim 500$ GeV. In the region around $\tan\beta \approx 5$ and $M_A \approx 300$ GeV, the dominance of the decays to EW-inos in the $M_h^{125}(\tilde{\chi})$ scenario reduces the sensitivity of the $\tau^+\tau^-$ channel, which explains the difference in the exclusion bounds from heavy-Higgs searches with respect to the M_h^{125} and $M_h^{125}(\tilde{\tau})$ scenarios – see Figs. 1 and 2, respectively – where this region is excluded by the LHC searches for $H/A \to \tau^+\tau^-$. However, we remark that this region is independently ruled out by the requirement that the lighter $\mathcal{CP}$-even scalar be sufficiently SM-like. A comparison between the left and right plots of Fig. 7 shows that the decays of the $\mathcal{CP}$-odd scalar follow patterns similar to those of the heavier $\mathcal{CP}$-even scalar in most of the (M_A , $\tan\beta$) plane. The

only exception is the corner with low $\tan\beta$ and M_A below the $t\bar{t}$ threshold, where H decays mostly to pairs of SM particles whereas A decays mostly to EW-ino pairs. The plots of Fig. 7 suggest that a sizable region of the parameter space of the $M_h^{125}(\tilde{\chi})$ scenario could be probed by dedicated searches for MSSM Higgs bosons decaying to EW-ino pairs. Very early studies of the discovery potential of those searches were presented in public notes by ATLAS [224], which considered two scenarios from Ref. [225], and by CMS [226,227]. However, we are not aware of any update taking into account the existing results of the LHC runs. We also remark that an eventual tightening of the bounds on the EW-ino masses could be easily compensated for by an increase in the values of M_1, M_2 and μ by about 100 GeV, without significantly affecting the decay rates of the heavy Higgs bosons in the allowed region with $M_A \gtrsim 600$ GeV. The main implication of such a modification of our scenario would be a smaller enhancement of the branching ratio for $h \to \gamma\gamma$ at low $\tan\beta$.

Finally, the left plot in Fig. 8 shows, in the $(M_A\,, \tan\beta)$ plane, the branching ratio for the decays of a charged Higgs boson $H^\pm$ to chargino–neutralino pairs in the $M_h^{125}(\tilde{\chi})$ scenario (again, a sum is taken over all of the allowed final states). A comparison with Fig. 7 shows that the decays of $H^\pm$ to EW-inos follow approximately the same pattern as the corresponding decays of the heavier $\mathcal{CP}$-even scalar, and can be the dominant ones for intermediate values of $\tan\beta$. The right plot in Fig. 8 shows instead the total rate (in fb) for the production of a charged Higgs boson in association with a top quark, followed by the decay to a chargino–neutralino pair, at the LHC with 13 TeV center-of-mass energy (a factor 2 is included to account for both Higgs charges). The plot suggests that, for the values of the charged-Higgs mass allowed in this scenario by the constraints on the neutral sector (say, $M_{H^\pm} \gtrsim 600$ GeV) and intermediate values of $\tan\beta$, the rates for top-associated production of $H^\pm$ followed by decays to EW-inos are comparable to those recently probed by ATLAS in the $\tau\nu$ channel with 36 fb^{-1} of Run-2 data [154]. Even considering the complications in the reconstruction of the subsequent EW-ino decays, we believe that a study of this scenario with the full Run-2 dataset would be well motivated.

In summary, as was discussed e.g. in Refs. [15,228–230], the presence of light EW-inos in the $M_h^{125}(\tilde{\chi})$ scenario lowers the sensitivity of the traditional searches for heavy Higgs bosons decaying to pairs of SM particles, especially in the region with intermediate $\tan\beta$, but opens up the possibility to probe the same region through the Higgs decays to SUSY particles. We propose these decays as a target of dedicated searches at the LHC.

3.6 Scenarios characterized by alignment without decoupling

In models with an extended Higgs sector, the so-called *alignment limit* [11,12,70–73] corresponds to the case in which one of the neutral $\mathcal{CP}$-even scalars is aligned in field space with the direction of the SM Higgs vev, and thus has SM-like couplings to gauge bosons and matter fermions. In a general 2HDM, such alignment is commonly associated with the *decoupling limit*, in which the lighter $\mathcal{CP}$-even scalar h is approximately SM-like and all the remaining Higgs states are significantly heavier. However, alignment can also arise *without decoupling* – i.e., irrespective of the Higgs mass spectrum – if the term in the mass matrix for the neutral $\mathcal{CP}$-even scalars that mixes the field aligned with the SM Higgs vev with the field orthogonal to it vanishes exactly. In this case, the role of the SM Higgs boson can be played by either of the two $\mathcal{CP}$-even scalars.

Alignment without decoupling can arise as a consequence of some global symmetry of the Higgs sector [231,232], or even of an extended supersymmetry [233–235]. In the MSSM, however, it can only arise from an accidental cancellation between the tree-level mixing term and the radiative corrections in the mass matrix, and is thus associated to rather specific choices of the SUSY parameters. As discussed in detail in Refs. [11,12,72,73], for values of μ/M_S and A_f/M_S of order one (where A_f denotes collectively the trilinear soft-SUSY-breaking couplings of the third-generation sfermions, and M_S denotes the scale of the corresponding sfermion masses) the required cancellation in the mass matrix can be achieved only for large values of $\tan\beta$. For example, we noted in Sect. 3.5.1 that the $M_h^{125}(\tilde{\tau})$ scenario features alignment without decoupling for $\tan\beta \approx 52$, thanks to radiative corrections involving stau loops. However, already for $\tan\beta \gtrsim 15$ the bounds from $\tau^+\tau^-$ searches at the Run 2 of the LHC allow only for masses of the additional Higgs bosons above one TeV, i.e. large enough to be well within the decoupling limit. To obtain alignment without decoupling for $\tan\beta \lesssim 8$, such that the $\tau^+\tau^-$ bounds allow for masses of the additional Higgs bosons below 500 GeV, the ratios μ/M_S and, in some cases, A_t/M_S must be increased to values of about 3 or even larger (in contrast, the couplings of staus and sbottoms become less relevant for moderate $\tan\beta$, as do the Δ_b effects).[5] While we are aware that such large values of μ/M_S and A_t/M_S are expected to be in conflict with the requirement of avoiding CCB minima of the scalar potential [199–204], we believe that the rich Higgs-sector phenomenology of alignment scenarios with moderate $\tan\beta$ still motivates their investigation at the LHC.

[5] Despite the large values of μ/M_S, in the relevant regions of our alignment scenarios we find $\Delta_b \approx 0.2$.

Benchmark scenarios for MSSM Higgs searches characterized by alignment without decoupling have already been proposed in the literature, but their viability has been investigated only with respect to the results of Higgs and SUSY searches at Run 1 of the LHC. In particular, Refs. [73,79] introduced a scenario named "$m_h^{\rm alt}$", in which alignment occurs for $\tan\beta \approx 10$ and the role of the SM-like Higgs boson with mass around 125 GeV is played by h. Ref. [11] introduced instead three variants of a scenario named "low-$M_H^{\rm alt}$" – themselves meant as updates of the original "low-M_H" scenario of Ref. [15] – in which alignment occurs for $\tan\beta \approx 6$–7, and the role of the observed Higgs boson is played by the heavier $\mathcal{CP}$-even scalar H (the Dark Matter phenomenology of alignment scenarios was subsequently investigated in Refs. [236,237]). An update of these alignment scenarios seems now in order, motivated both by the improvements in the predictions for Higgs masses and couplings implemented in `FeynHiggs` and by the tightening of the experimental constraints on the relevant MSSM parameters in view of the available Run-2 results.

In this section we present two new benchmark scenarios characterized by alignment without decoupling at relatively low values of $\tan\beta$. In the first scenario the role of the observed Higgs boson is played by h, whereas in the second scenario – which requires somewhat extreme parameter choices and is already highly constrained (but not ruled out) by the available LHC searches – that role is played by H.

3.6.1 M_h^{125}(alignment) *scenario*

In this scenario the SUSY input parameters are fixed as

$$\begin{aligned} &M_{Q_3} = M_{U_3} = M_{D_3} = 2.5\ \text{TeV}, \quad M_{L_3} = M_{E_3} = 2\ \text{TeV}, \\ &\mu = 7.5\ \text{TeV}, \quad M_1 = 500\ \text{GeV}, \quad M_2 = 1\ \text{TeV}, \\ &M_3 = 2.5\ \text{TeV}, A_t = A_b = A_\tau = 6.25\ \text{TeV}. \end{aligned} \tag{7}$$

In order to obtain both alignment without decoupling and an acceptable prediction for M_h for $\tan\beta \lesssim 8$, the parameters that determine the stop masses take significantly larger values than in the scenarios defined in Sects. 3.4 and 3.5. We also remark that the stop mixing parameter $X_t = A_t - \mu\cot\beta$ is not fixed to a constant value over the considered parameter space, and, due to the large value of μ, shows a significant dependence on $\tan\beta$. The trilinear coupling A_t is chosen in such a way that the prediction for M_h is maximized around the value of $\tan\beta$ for which the alignment behavior occurs. In contrast, the specific choice of the gaugino mass parameters M_1 and M_2 is rather irrelevant to the phenomenology of this scenario, because the large value of μ implies a small mixing between the lighter gaugino-like EW-inos and the heavier higgsino-like EW-inos. Hence, even if M_1 and M_2 were smaller and Higgs-boson decays to EW-inos were kinematically allowed at lower values of M_A, their rates would be strongly suppressed by small couplings.

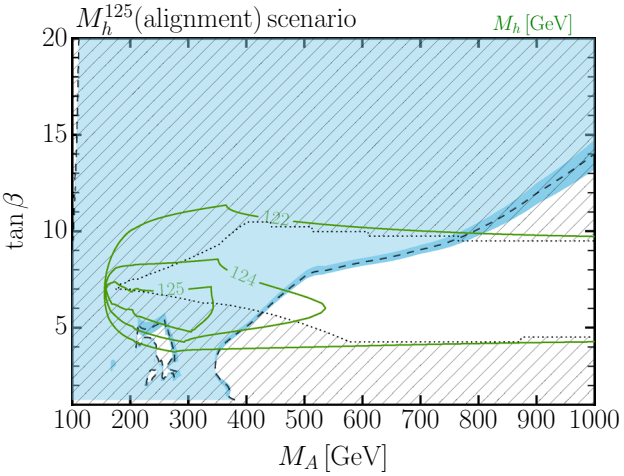

Fig. 9 Constraints on the M_h^{125}(alignment) scenario from Higgs searches at the LHC, in the (M_A , $\tan\beta$) plane. The green solid lines are predictions for the mass of the lighter $\mathcal{CP}$-even scalar h, the hatched area is excluded by a mismatch between the properties of h and those of the observed Higgs boson, and the blue area is excluded by the searches for additional Higgs bosons (the darker-blue band shows the theoretical uncertainty of the exclusion)

In Fig. 9 we present the existing constraints on the M_h^{125}(alignment) scenario from Higgs boson searches at the LHC, in the (M_A , $\tan\beta$) plane. To highlight the alignment effects, we focus on the region with 100 GeV $\leq M_A \leq$ 1 TeV and $1 \leq \tan\beta \leq 20$. The green solid lines show that, as a result of the dependence of X_t on $\tan\beta$, the mass of the lighter $\mathcal{CP}$-even scalar is maximized for $\tan\beta \approx 6$. The decrease of M_h with increasing M_A, which contrasts with the usual tree-level behavior, originates from two-loop diagrams involving squarks and a heavy Higgs boson.[6]

The shape of the hatched region ruled out by `HiggsSignals` shows that, in this scenario, the limit of alignment without decoupling is realized for $\tan\beta \approx 7$. Indeed, around this value of $\tan\beta$ we see a wedge-shaped region in which the lighter $\mathcal{CP}$-even scalar can be identified with the observed Higgs boson for values of M_A as low as 170 GeV. When M_A increases, the allowed region opens up towards both smaller and larger values of $\tan\beta$, as a consequence of the usual decoupling behavior. However, even at large values of M_A the requirement that M_h be compatible with the measured Higgs mass (within the theoretical uncertainty of the MSSM prediction) limits the allowed region to the band in which $4 \lesssim \tan\beta \lesssim 10$.

Finally, the blue region ruled out by the searches for heavy Higgs bosons at the LHC, as determined by `HiggsBounds`,

[6] In view of the large hierarchy between the respective masses, a resummation of terms enhanced by powers of $\ln(M_S/M_A)$ may be necessary for $M_A \lesssim 500$ GeV, but that is not yet implemented in `FeynHiggs`.

is similar to the corresponding regions in the M_h^{125} and $M_h^{125}(\tilde{\tau})$ scenarios, see Figs. 1 and 2, respectively. We see that a large portion of the wedge where alignment occurs without decoupling is already excluded. However, we remark that the lowest value of M_A allowed in this scenario by both the heavy-Higgs searches and the constraints on the properties of the lighter $\mathcal{CP}$-even scalar, which is about 430 GeV, is still significantly lower than the bound of about 600 GeV found in the first three scenarios.

3.6.2 M_H^{125} scenario

MSSM scenarios in which the role of the SM-like Higgs boson is played by the heavier $\mathcal{CP}$-even scalar H are constrained by the fact that the masses of all Higgs states are typically below 200 GeV, thus the searches for additional (neutral or charged) Higgs bosons at the LHC already rule out most of the available parameter space. Earlier proposals for such scenarios [11,15] focused on the region with $M_{H^\pm} \approx m_t$ and low $\tan\beta$, triggered by the fact that no search for charged Higgs bosons had yet been performed in that region due to the lack of accurate predictions for the signal, and that the region was not yet ruled out by the searches for neutral Higgs bosons decaying to tau pairs. Recently, the ATLAS collaboration published a search for charged Higgs bosons [154] that covers the full range of 90 GeV $\leq M_{H^\pm} \leq$ 2 TeV, employing the NLO predictions of Ref. [127] for the total cross section for charged-Higgs production with $M_{H^\pm} \approx m_t$. However, in that region the ATLAS search does not yet rule out low values of $\tan\beta$. Moreover, the ATLAS search assumes that the charged Higgs boson decays only through $H^\pm \to \tau^\pm\nu$, whereas in scenarios where H is SM-like the channel $H^\pm \to W^\pm h$ may become dominant when it is kinematically open. It therefore seems worthwhile to devise a benchmark scenario in which alignment without decoupling occurs for $\tan\beta \approx$ 5–6, and H is approximately SM-like in the region that has not been covered so far by the charged-Higgs searches.

The M_H^{125} scenario is defined by the following input parameters:

$$
\begin{aligned}
&M_{Q_3} = M_{U_3} = 750\,\text{GeV} - 2\,(M_{H^\pm} - 150\,\text{GeV})\,,\\
&\mu = [5800\,\text{GeV} + 20\,(M_{H^\pm} - 150\,\text{GeV})]\; M_{Q_3}/(750\,\text{GeV})\,,\\
&A_t = A_b = A_\tau = 0.65\,M_{Q_3}, \quad M_{D_3} = M_{L_3} = M_{E_3} = 2\,\text{TeV},\\
&M_1 = M_{Q_3} - 75\,\text{GeV}, \quad M_2 = 1\,\text{TeV}, \quad M_3 = 2.5\,\text{TeV}. \qquad (8)
\end{aligned}
$$

To make the interplay with the charged-Higgs searches more transparent, the free parameters in this scenario are chosen as $\tan\beta$ and $M_{H^\pm}$, with the latter varied between 150 and 200 GeV. In contrast with the scenarios discussed earlier, the parameters that determine the stop masses and couplings and the LSP mass are varied as a function of $M_{H^\pm}$, in order to maximize the experimentally viable parameter space. In particular, the decrease of the stop masses with increasing

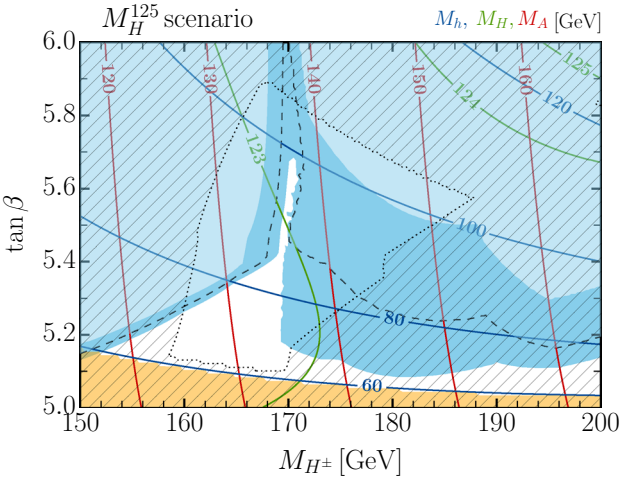

Fig. 10 Constraints on the M_H^{125} scenario from Higgs searches at the LHC, in the $(M_{H^\pm}, \tan\beta)$ plane. The blue, green and red solid lines are predictions for the masses of h, H and A, respectively. The hatched area is excluded by a mismatch between the properties of H and those of the observed Higgs boson, and the areas bounded by dashed lines are excluded by the searches for additional Higgs bosons (the darker-blue band shows the theoretical uncertainty of the exclusion). At low $\tan\beta$, the orange area is excluded by searches for $H \to hh$

$M_{H^\pm}$ has the purpose of delaying the crossing point at which h becomes SM-like and M_H starts growing with $M_{H^\pm}$. The soft-SUSY-breaking bino mass M_1 is varied together with the stop masses in order to ensure a compressed squark-neutralino spectrum, still compatible with the existing mono-jet searches [39,40] in the region of the parameter space that is not excluded by other constraints. Finally, the parameter μ takes particularly large values, about 8–9 times the stop masses, to ensure that alignment occurs at values of $\tan\beta$ low enough to evade the bounds from $H/A \to \tau^+\tau^-$ searches. Once again, we acknowledge the possible tension with the theoretical bounds from the stability of the scalar potential.

In Fig. 10 we present the existing constraints on the M_H^{125} scenario from Higgs searches at the LHC, in the relevant region of the $(M_{H^\pm}, \tan\beta)$ plane. The blue, green and red solid lines represent the masses of h, H and A, respectively, and the meaning of the hatched and blue regions is the same as in Fig. 1. The figure shows that, although the M_H^{125} scenario is already strongly constrained, a small region in which H can be identified with the observed Higgs boson is still allowed. In particular, the widest spread in $\tan\beta$ is obtained for $M_{H^\pm} \approx$ 170 GeV, where $\tan\beta$ ranges between 5.1 and 5.8, while the widest spread in $M_{H^\pm}$ is obtained for $\tan\beta \approx$ 5.3, where $M_{H^\pm}$ ranges between 160 GeV and 175 GeV.

The non-hatched region allowed by `HiggsSignals` is roughly shaped as an irregular quadrilateral. We remark that this shape results from a non-trivial interplay between the contributions of different Higgs bosons to the signal strengths that `HiggsSignals` compares with the ATLAS and CMS

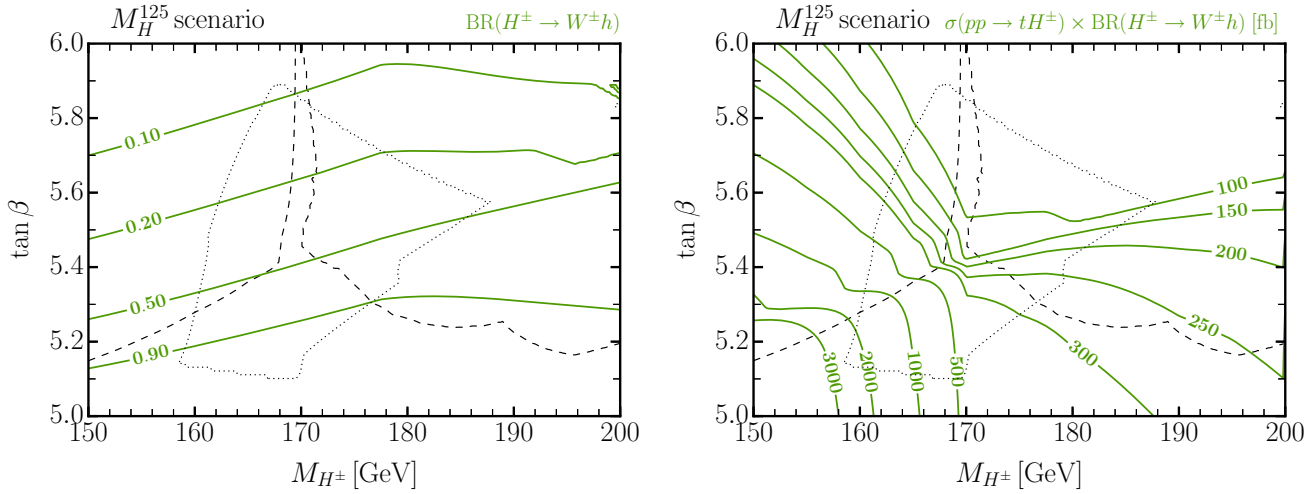

Fig. 11 Left: Branching ratio for the decay $H^\pm \to W^\pm h$ as a function of $M_{H^\pm}$ and $\tan\beta$ in the M_H^{125} scenario. Right: Total rate (in fb) for the production of a charged Higgs boson in association with a top quark, followed by the decay to a $W^\pm h$ pair, at the LHC with 13 TeV center-of-mass energy. In each plot, the boundaries of the exclusion regions from Fig. 10 are shown as a dashed and a dotted black line, respectively

measurements.[7] In parts of the allowed region, the decays $H \to b\bar{b}$ and $H \to \tau^+\tau^-$ are somewhat suppressed with respect to the SM prediction. However, since a mass resolution of 20 GeV is assumed for the corresponding measurements, the suppression can be compensated for by the contribution of the $\mathcal{CP}$-odd scalar A (this explains the step-like feature in the border of the allowed region at $M_{H^\pm} \approx 179$ GeV, where $M_A \approx 145$ GeV). On the other hand, when $M_h \gtrsim 105$ GeV the decays $h \to b\bar{b}$ and $h \to \tau^+\tau^-$ (as well as the associated production of h with top quarks) also start contributing to the signal strengths, ruling out a region in which H itself would be fairly SM-like. For decreasing $\tan\beta$, radiative corrections to the $\mathcal{CP}$-even scalar mass matrix that are enhanced by the large value of μ induce a sharp decrease in the mass of the lighter eigenstate h. The lower edge of the region allowed by `HiggsSignals` lies where M_h becomes lower than $M_H/2$ and the decay $H \to hh$ opens up, suppressing the branching ratios of the SM-like decays of H. The strip in which M_h ranges between roughly 25 and 60 GeV is also constrained by direct searches for the decays of the 125-GeV Higgs boson to pairs of light scalars. In particular, the region excluded by the Run-1 CMS search for the decay channel $H \to hh \to b\bar{b}\,\mu^+\mu^-$ [148] is shown in orange in Fig. 10.

As shown by the areas bounded by dashed lines, the searches for additional Higgs bosons implemented in `HiggsBounds` cut parts of the non-hatched region allowed by `HiggsSignals`. In particular, the region with $M_{H^\pm} \lesssim 170$ GeV is excluded by the ATLAS search for charged Higgs bosons decaying via $H^\pm \to \tau^\pm\nu$ [154], down to values of $\tan\beta$ for which the decay channel $H^\pm \to W^\pm h$ becomes dominant. The region with $M_{H^\pm} \gtrsim 170$ GeV and $\tan\beta \gtrsim 5.3$–5.4 is instead excluded by the CMS searches for $A \to \tau^+\tau^-$ [138,139]. However, the two exclusion regions do not overlap, leaving a narrow unexcluded strip around $M_{H^\pm} \approx 170$ GeV which extends up to the edge of the region allowed by `HiggsSignals`. We also note that the theoretical uncertainty of the exclusion region at larger $M_{H^\pm}$, shown as a darker-blue area in Fig. 10, is far from negligible, because the rate for the process $pp \to A \to \tau^+\tau^-$ varies rather mildly over the considered range of $\tan\beta$. In particular, the use of the lowest estimates for the production cross sections of the neutral Higgs bosons would significantly weaken the bound from the $A \to \tau^+\tau^-$ searches, extending the allowed region up to $M_{H^\pm} \approx 185$ GeV.

Finally, we show in the left plot of Fig. 11 the branching ratio for the decay of a charged Higgs boson to a W boson and the lighter $\mathcal{CP}$-even scalar h in the M_H^{125} scenario, and in the right plot of Fig. 11 the total rate (in fb) for the production of a charged Higgs boson in association with a top quark, followed by the decay to a $W^\pm h$ pair, at the LHC with 13 TeV center-of-mass energy (a factor 2 is included to account for both Higgs charges). The left plot shows that, in the bulk of the allowed region where $\tan\beta \lesssim 5.4$, the decay channel $H^\pm \to W^\pm h$ is indeed the dominant one (with the non-SM-like h in turn decaying mostly to bottom quarks or taus). The right plot suggests instead that, in this region, the total rate for the process $pp \to tH^\pm \to t(W^\pm h)$ lies roughly between 200 fb and 2 pb, making this process an appealing candidate for a novel charged-Higgs search at the LHC.

[7] We stress again that these features depend to some extent on the way the ATLAS and CMS results are implemented in `HiggsSignals`, and that dedicated analyses of the M_H^{125} scenario by the experimental collaborations would certainly yield more-accurate exclusion profiles.

3.7 $M_{h_1}^{125}$(CPV) scenario

Our sixth benchmark scenario, denoted as the "$M_{h_1}^{125}$(CPV) scenario", is characterized by $\mathcal{CP}$ violation in the Higgs sector, and provides an illustration of the interference effects in Higgs production and decays discussed in Sect. 2.3. The relevant parameters are chosen such that the strongest interference region is located near the exclusion contour of the corresponding scenario with real parameters, the mass of the SM-like scalar is near the observed value, and all EDMs are within the allowed ranges. Our scenario can be considered a minimal $\mathcal{CP}$-violating setup, in that the violation occurs as a result of a single non-zero phase for the soft-SUSY-breaking Higgs-stop interaction term, defined as $A_t \equiv |A_t|\, e^{i\phi_{A_t}}$. We choose a non-zero ϕ_{A_t} because this phase affects the Higgs sector already at one loop, via the dominant corrections controlled by the large top Yukawa coupling, while being the least constrained by EDMs. Indeed, the other relevant phases[8] ϕ_{A_f} (with $f \neq t$), ϕ_{M_1}, ϕ_{M_3} and ϕ_μ induce smaller effects and/or are more severely constrained (see, e.g., Refs. [238–240] for discussions of EDM constraints in the MSSM).

In the $M_{h_1}^{125}$(CPV) scenario the SUSY input parameters are fixed as

$$\begin{aligned} &M_{Q_3} = M_{U_3} = M_{D_3} = M_{L_3} = M_{E_3} = 2\ \text{TeV}, \\ &\mu = 1.65\ \text{TeV}, \quad M_1 = M_2 = 1\ \text{TeV}, \quad M_3 = 2.5\ \text{TeV}, \\ &|A_t| = \mu \cot\beta + 2.8\ \text{TeV}, \quad \phi_{A_t} = \frac{2\pi}{15}, \quad A_b = A_\tau = |A_t|. \end{aligned} \tag{9}$$

The non-zero phase ϕ_{A_t} leads to an admixture among the neutral $\mathcal{CP}$-even scalars, h and H, and the $\mathcal{CP}$-odd scalar, A, into the loop-corrected mass eigenstates h_1, h_2 and h_3. Since A is not a mass eigenstate, the charged-Higgs mass $M_{H^\pm}$ is used as a free input parameter together with $\tan\beta$. In scans over the $(M_{H^\pm}, \tan\beta)$ plane, $\tan\beta$ can be varied between 1 and 20, and $M_{H^\pm}$ between 120 GeV and 1 TeV (to highlight the interference effects, we focus on a smaller region of the parameter space than in the scenarios of Sects. 3.4 and 3.5). As in the M_h^{125} scenario defined in section 3.4, the mass parameters for all SUSY particles are chosen to be so large that production and decays of the MSSM Higgs bosons are only mildly affected by their presence. The largest loop-induced SUSY effect arises through the Δ_b correction, which takes on values similar to those in the M_h^{125} scenario. We also remark that, in contrast to the scenarios defined in Sects. 3.4 and 3.5, the stop mixing parameter $X_t = A_t - \mu \cot\beta$ is not fixed to a constant value over the considered parameter space. However, for our choices of A_t and μ the residual dependence of X_t on $\tan\beta$ has only a very small effect on the stop masses when $\tan\beta \gtrsim 5$.

[8] In fact, only the phases of various products of Lagrangian parameters are independent from each other. With appropriate field redefinitions, we can assume M_2 and the soft-SUSY-breaking Higgs mixing term B_μ to be real without loss of generality.

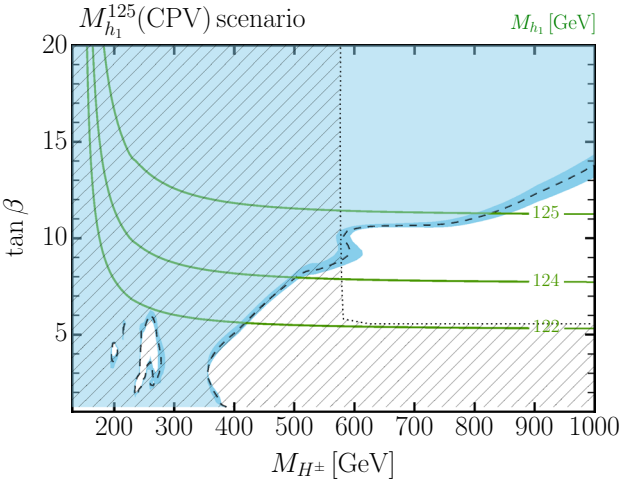

Fig. 12 Constraints on the $M_{h_1}^{125}$(CPV) scenario from Higgs searches at the LHC, in the $(M_{H^\pm}, \tan\beta)$ plane. The green solid lines are predictions for the mass of the lightest neutral scalar h_1, the hatched area is excluded by a mismatch between the properties of h_1 and those of the observed Higgs boson, and the blue area is excluded by the searches for additional Higgs bosons (the darker-blue band shows the theoretical uncertainty of the exclusion)

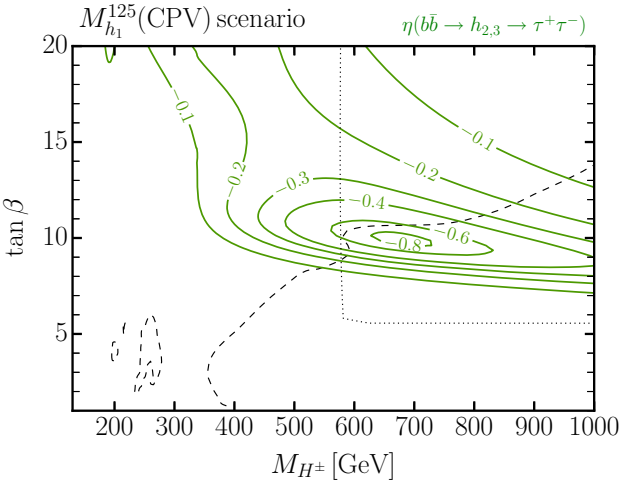

Fig. 13 The same exclusion boundaries as in Fig. 12 above are overlaid with contours of the relative interference factor $\eta(b\bar{b} \to h_{2,3} \to \tau^+\tau^-)$ defined in Eq. (2)

In Fig. 12 we present, in the $(M_{H^\pm}, \tan\beta)$ plane, the existing constraints on the $M_{h_1}^{125}$(CPV) scenario from Higgs-boson searches at the LHC. The meaning of the blue and hatched exclusion regions is the same as in Fig. 1, but the green solid lines refer here to the mass of the lightest mass eigenstate h_1. The plot shows that M_{h_1} takes on slightly larger values in the $M_{h_1}^{125}$(CPV) scenario than M_h does in the M_h^{125} scenario, due to the different choices for the soft-SUSY-breaking stop masses and for X_t. The hatched region excluded by the requirement that the properties of the lightest

scalar match those of the observed Higgs boson is qualitatively similar to the corresponding region in the M_h^{125} scenario, see Fig. 1. In contrast, the contour of the blue region excluded by the LHC searches for the heavier scalars h_2 and h_3 differs markedly from the corresponding contour in Fig. 1, with a "bay"-shaped allowed region opening up around $M_{H^\pm} \approx 650$ GeV and $\tan\beta \approx 10$, where the most sensitive searches are the ones for $h_2/h_3 \to \tau^+\tau^-$.

To elucidate the origin of this feature, Fig. 13 shows the relative interference factor for the production of the heavier states h_2 and h_3 in bottom-quark annihilation followed by their decay to a $\tau^+\tau^-$ pair, i.e. the factor $\eta(b\bar{b} \to h_{2,3} \to \tau^+\tau^-)$ defined in Eq. (2). The interference factor for the gluon-fusion process – which is very similar to the one for bottom-quark annihilation – has also been taken into account in the evaluation of the exclusion region with `HiggsBounds`. However, the interference effect for bottom-quark annihilation is the one with the strongest impact on the exclusion contour, due to the larger cross section for intermediate to large values of $\tan\beta$. The plot clearly demonstrates that the unexcluded "bay" corresponds to a region where a large destructive interference reduces the prediction for the combined rate of h_2 and h_3 to less than about 30% of the value that one would obtain by neglecting the interference effects (in fact, the minimal rate at the center of the interference region corresponds to just 4% of the value without interference). In this region the mixing of the neutral $\mathcal{CP}$-even scalar h with the heavier states is negligible, while the mass eigenstates h_2 and h_3 are strong admixtures of the $\mathcal{CP}$ eigenstates H and A, and they are almost degenerate in mass.

The unconventional shape of the exclusion contour highlights the importance of taking Higgs interference effects into account in $\mathcal{CP}$-violating scenarios: even with the full luminosity of Run 2 of the LHC, it is possible that ATLAS and CMS will not be able to completely rule out the region of the $M_{h_1}^{125}$(CPV) scenario in which the heavy-Higgs rates are reduced by up to one order of magnitude with respect to the corresponding rates in the $\mathcal{CP}$-conserving case. Moreover, we stress again that the occurrence of a sizable negative interference is a rather universal feature of such $\mathcal{CP}$-violating scenarios. Even if the region of the $M_{h_1}^{125}$(CPV) scenario where the strongest interference arises should eventually be ruled out by tightening experimental constraints, one should note that a slight change of parameters would shift that region to larger $H^\pm$ masses and/or lower values of $\tan\beta$, while still yielding M_{h_1} near the observed value and fulfilling the EDM constraints. At larger $M_{H^\pm}$, viable interference regions require larger ϕ_{A_t} in combination with either larger μ or a larger constant term in the prescription for $|A_t|$, see Eq. (9), and lower μ. At lower $\tan\beta$, they can instead be obtained by reducing ϕ_{A_t} and increasing the constant term for $|A_t|$.

Finally, we checked with `FeynHiggs` and `CPsuperH` that the relevant interference region of the $M_{h_1}^{125}$(CPV) scenario is compatible with the bounds on the most sensitive EDMs, which in this case are the EDMs of the electron and the neutron. The strongest constraint arises from the upper bound on the electron EDM [51], whereas in case of a non-vanishing phase of M_3 the neutron EDM [50] would be very restrictive. Due to the enhancement of the electron EDM for larger $\tan\beta$ and smaller Higgs masses, the upper-left corner of the $(M_{H^\pm}, \tan\beta)$ plane in Fig. 12 is in fact excluded by the electron EDM, but only in a region that is also excluded by the direct searches for heavy Higgs bosons.

4 Conclusions

In this paper we have proposed six new benchmark scenarios for MSSM Higgs boson searches at the LHC. Our scenarios are expressed in terms of TeV-scale parameters, chosen to illustrate different aspects of Higgs phenomenology in the MSSM. They include one case with complex parameters, but they all assume R-parity conservation and no flavor mixing. The scenarios are compatible – at least over wide portions of their parameter space – with the most recent LHC results for the Higgs-boson properties and the bounds on masses and couplings of new particles. Each scenario contains one $\mathcal{CP}$-even scalar with mass around 125 GeV and SM-like couplings. For each scenario we have investigated the impact on the parameter space of the current exclusion bounds from Higgs searches at LEP, the Tevatron and the LHC, taking both experimental and theory uncertainties into account.

Our first scenario, "M_h^{125}", is characterized by relatively heavy superparticles, so the Higgs phenomenology at the LHC resembles that of a 2HDM with MSSM-inspired Higgs couplings. The second and third scenario, "$M_h^{125}(\tilde{\tau})$" and "$M_h^{125}(\tilde{\chi})$", are characterized by some of the superparticles – staus and EW-inos, respectively – being relatively light. This affects the decays of the heavier Higgs bosons, weakening the exclusion bounds from the $\tau^+\tau^-$ searches, as well as the decay of the lighter $\mathcal{CP}$-even scalar to photons. On the other hand, the possibility to look for additional Higgs bosons through their decays to EW-inos opens up. The fourth and fifth scenario are characterized by the phenomenon of "alignment without decoupling", in which one of the two neutral $\mathcal{CP}$-even scalars has SM-like couplings independently of the mass spectrum of the remaining Higgs bosons. In particular, our fourth scenario, "M_h^{125}(alignment)", features a lighter $\mathcal{CP}$-even scalar with SM-like couplings for $\tan\beta \approx 7$, independently of the heavy Higgs-boson mass scale. It is thus naturally in agreement with the measurements of the Higgs-boson properties at the LHC also for relatively low values of M_A. In the fifth scenario, "M_H^{125}", the heavier $\mathcal{CP}$-even scalar is the one with mass around 125 GeV and SM-like

couplings. In this scenario all Higgs bosons are relatively light, posing very strong experimental bounds on the parameter space. Nevertheless, the scenario appears to be viable for $\tan\beta \approx 5-6$ and very large values of μ, and also features the novel signature of a relatively light charged Higgs boson decaying to a W boson and the lighter $\mathcal{CP}$-even scalar. Finally, the sixth scenario, "$M_{h_1}^{125}$(CPV)", incorporates $\mathcal{CP}$ violation in the Higgs sector and gives rise to a strong admixture of the two heavier neutral states, leading to significant interference effects in their production and decay which weaken the exclusion bounds from $\tau^+\tau^-$ searches.

Spanning a wide variety of MSSM Higgs-boson phenomenology, we hope that these new benchmark scenarios can serve as a guideline and motivation for upcoming LHC searches for additional neutral and charged Higgs bosons.

Note added

The recent improvement of the upper bound on the electron EDM of the ACME collaboration [241] excludes the phase ϕ_{A_t} used in the $M_{h_1}^{125}$(CPV) scenario, unless one invokes subtle cancellations between different contributions to the EDM. However, from our point of view such a scenario with two overlapping, interfering Higgs-boson signals is still of interest. First, for smaller phases compatible with newest EDM bounds the interference effects are obviously smaller, but would still need to be taken into account for a proper exclusion or discovery of heavier Higgs bosons. It thus seems useful to study the relevance of such effects in a scenario where they are clearly visible. Second, such interferences can be considered as a first step towards an implementation of (experimentally non-resolvable) Higgs signal and background interferences, which will be relevant in single-Higgs production as well as in other channels (e.g. $t\bar{t}$, Ah or hh) with increasing integrated luminosity.

Acknowledgements This work was initiated in the context of the activities of the LHC-HXSWG, and some of our findings were presented in a preliminary form at recent meetings of the group. We thank F. Staub for his help concerning the usage of `Vevacious`, L. Shang for communications about `CheckMATE`, and F. Domingo, S. Paßehr and J. Wittbrodt for helpful discussions. E. F. is supported by the Minerva foundation. The work of S. H. is supported in part by the MEINCOP Spain under contract FPA2016-78022-P, in part by the Spanish "Agencia Estatal de Investigación" (AEI) and the EU "Fondo Europeo de Desarrollo Regional" (FEDER) through the project FPA2016-78022-P, and in part by the AEI through the grant IFT Centro de Excelencia Severo Ochoa SEV-2016-0597. The work of P. S. is supported in part by the French "Agence Nationale de la Recherche" (ANR), in the context of the LABEX ILP (ANR-11-IDEX-0004-02, ANR-10-LABX-63) and of the grant "HiggsAutomator" (ANR-15-CE31-0002). P. S. also acknowledges support by the Research Executive Agency (REA) of the European Commission under the Initial Training Network "HiggsTools" (PITN-GA-2012-316704) and by the European Research Council (ERC) under the Advanced Grant "Higgs@LHC" (ERC-2012-ADG_20120216-321133). T. S. acknowledges support from the DESY Fellowship programme. The work of C. W. at University of Chicago is supported in part by U.S. Department of Energy grant number DE-FG02-13ER41958, and his work at ANL is supported in part by the U.S. Department of Energy under Contract No. DE-AC02-06CH11357. C. W. would also like to thank the Aspen Center for Physics, which is supported by National Science Foundation grant PHY-1607611, for the kind hospitality during the completion of this work. G. W. acknowledges support by Deutsche Forschungsgemeinschaft through the SFB 676 "Particles, Strings and the Early Universe".

Data Availability Statement This manuscript has associated data in a data repository. [Authors' comment: The Higgs-boson masses, cross sections and branching ratios throughout the parameter planes of our benchmark scenarios are available in the form of `ROOT` files on the web page of the MSSM subgroup of the LHC-HXSWG.]

References

1. ATLAS Collaboration, G. Aad et al., Observation of a new particle in the search for the Standard Model Higgs boson with the ATLAS detector at the LHC. Phys. Lett. B **716**, 1–29 (2012). arXiv:1207.7214 [hep-ex]
2. CMS Collaboration, S. Chatrchyan et al., Observation of a new boson at a mass of 125 GeV with the CMS experiment at the LHC. Phys. Lett. B **716**, 30–61 (2012). arXiv:1207.7235 [hep-ex]
3. ATLAS, CMS Collaboration, G. Aad et al., Combined measurement of the Higgs Boson mass in pp collisions at $\sqrt{s} = 7$ and 8 TeV with the ATLAS and CMS experiments. Phys. Rev. Lett. **114**, 191803 (2015). arXiv:1503.07589 [hep-ex]
4. ATLAS, CMS Collaboration, G. Aad et al., Measurements of the Higgs boson production and decay rates and constraints on its couplings from a combined ATLAS and CMS analysis of the LHC pp collision data at $\sqrt{s} = 7$ and 8 TeV. JHEP **08**, 045 (2016). arXiv:1606.02266 [hep-ex]
5. H.P. Nilles, Supersymmetry, supergravity and particle physics. Phys. Rep. **110**, 1–162 (1984)
6. H.E. Haber, G.L. Kane, The search for supersymmetry: probing physics beyond the standard model. Phys. Rep. **117**, 75–263 (1985)
7. J.F. Gunion, H.E. Haber, Higgs Bosons in supersymmetric models. 1. Nucl. Phys. B **272**, 1 (1986) [**Erratum: Nucl. Phys. B 402, 567 (1993)**]
8. P. Draper, H. Rzehak, A review of Higgs mass calculations in supersymmetric models. Phys. Rep. **619**, 1–24 (2016). arXiv:1601.01890 [hep-ph]
9. S. Heinemeyer, O. Stål, G. Weiglein, Interpreting the LHC Higgs search results in the MSSM. Phys. Lett. B **710**, 201–206 (2012). arXiv:1112.3026 [hep-ph]
10. P. Bechtle, S. Heinemeyer, O. Stål, T. Stefaniak, G. Weiglein, L. Zeune, MSSM interpretations of the LHC discovery: light or heavy Higgs? Eur. Phys. J. C **73**(4), 2354 (2013). arXiv:1211.1955 [hep-ph]
11. P. Bechtle, H.E. Haber, S. Heinemeyer, O. Stål, T. Stefaniak, G. Weiglein, L. Zeune, The light and heavy Higgs interpretation of the MSSM. Eur. Phys. J. C **77**(2), 67 (2017). arXiv:1608.00638 [hep-ph]

12. H.E. Haber, S. Heinemeyer, T. Stefaniak, The impact of two-loop effects on the scenario of MSSM Higgs alignment without decoupling. Eur. Phys. J. C **77**(11), 742 (2017)
13. M. Carena, S. Heinemeyer, C.E.M. Wagner, G. Weiglein, Suggestions for improved benchmark scenarios for Higgs boson searches at LEP-2, in *Workshop on New Theoretical Developments for Higgs Physics at LEP-2 Geneva, Switzerland, October 27, 1999* (1999). arXiv:hep-ph/9912223 [hep-ph]
14. M. Carena, S. Heinemeyer, C.E.M. Wagner, G. Weiglein, Suggestions for benchmark scenarios for MSSM Higgs boson searches at hadron colliders. Eur. Phys. J. C **26**, 601–607 (2003). arXiv:hep-ph/0202167
15. M. Carena, S. Heinemeyer, O. Stål, C.E.M. Wagner, G. Weiglein, MSSM Higgs Boson searches at the LHC: benchmark scenarios after the discovery of a Higgs-like particle. Eur. Phys. J. C **73**(9), 2552 (2013). arXiv:1302.7033 [hep-ph]
16. M. Carena, J.R. Ellis, A. Pilaftsis, C.E.M. Wagner, CP violating MSSM Higgs bosons in the light of LEP-2. Phys. Lett. B **495**, 155–163 (2000). arXiv:hep-ph/0009212
17. M. Carena, J. Ellis, J.S. Lee, A. Pilaftsis, C.E.M. Wagner, CP violation in heavy MSSM Higgs scenarios. JHEP **02**, 123 (2016). arXiv:1512.00437 [hep-ph]
18. LHC Higgs Cross Section Working Group Collaboration, S. Heinemeyer et al., Handbook of LHC Higgs cross sections: 3. Higgs properties (2013). arXiv:1307.1347 [hep-ph]
19. LHC Higgs Cross Section Working Group Collaboration, D. de Florian et al., Handbook of LHC Higgs cross sections: 4. Deciphering the nature of the Higgs sector (2016). arXiv:1610.07922 [hep-ph]
20. T. Hahn, S. Heinemeyer, W. Hollik, H. Rzehak, G. Weiglein, High-precision predictions for the light CP-even Higgs Boson mass of the minimal supersymmetric standard model. Phys. Rev. Lett. **112**(14), 141801 (2014). arXiv:1312.4937 [hep-ph]
21. P. Draper, G. Lee, C.E.M. Wagner, Precise estimates of the Higgs mass in heavy supersymmetry. Phys. Rev. D **89**(5), 055023 (2014). arXiv:1312.5743 [hep-ph]
22. E. Bagnaschi, G.F. Giudice, P. Slavich, A. Strumia, Higgs mass and unnatural supersymmetry. JHEP **09**, 092 (2014). arXiv:1407.4081 [hep-ph]
23. J. Pardo Vega, G. Villadoro, SusyHD: Higgs mass determination in supersymmetry. JHEP **07**, 159 (2015). arXiv:1504.05200 [hep-ph]
24. H. Bahl, W. Hollik, Precise prediction for the light MSSM Higgs boson mass combining effective field theory and fixed-order calculations. Eur. Phys. J. C **76**(9), 499 (2016). arXiv:1608.01880 [hep-ph]
25. P. Athron, J. Park, T. Steudtner, D. Stöckinger, A. Voigt, Precise Higgs mass calculations in (non-)minimal supersymmetry at both high and low scales. JHEP **01**, 079 (2017). arXiv:1609.00371 [hep-ph]
26. F. Staub, W. Porod, Improved predictions for intermediate and heavy Supersymmetry in the MSSM and beyond. Eur. Phys. J. C **77**(5), 338 (2017). arXiv:1703.03267 [hep-ph]
27. E. Bagnaschi, J. Pardo Vega, P. Slavich, Improved determination of the Higgs mass in the MSSM with heavy superpartners. Eur. Phys. J. C **77**(5), 334 (2017). arXiv:1703.08166 [hep-ph]
28. H. Bahl, S. Heinemeyer, W. Hollik, G. Weiglein, Reconciling EFT and hybrid calculations of the light MSSM Higgs-boson mass. Eur. Phys. J. C **78**(1), 57 (2018). arXiv:1706.00346 [hep-ph]
29. B.C. Allanach, A. Voigt, Uncertainties in the lightest CP even Higgs Boson mass prediction in the minimal supersymmetric standard model: fixed order versus effective field theory prediction. Eur. Phys. J. C **78**(7), 573 (2018). arXiv:1804.09410 [hep-ph]
30. R.V. Harlander, J. Klappert, A.D. Ochoa Franco, A. Voigt, The light CP-even MSSM Higgs mass resummed to fourth logarithmic order (2018). arXiv:1807.03509 [hep-ph]
31. KUTS workshop series. https://sites.google.com/site/kutsmh/home
32. S. Heinemeyer, W. Hollik, G. Weiglein, FeynHiggs: a program for the calculation of the masses of the neutral CP even Higgs bosons in the MSSM. Comput. Phys. Commun. **124**, 76–89 (2000). arXiv:hep-ph/9812320
33. M. Frank, T. Hahn, S. Heinemeyer, W. Hollik, H. Rzehak, G. Weiglein, The Higgs Boson masses and mixings of the complex MSSM in the Feynman-diagrammatic approach. JHEP **02**, 047 (2007). arXiv:hep-ph/0611326
34. S. Heinemeyer, W. Hollik, G. Weiglein, The masses of the neutral CP- even Higgs bosons in the MSSM: accurate analysis at the two loop level. Eur. Phys. J. C **9**, 343–366 (1999). arXiv:hep-ph/9812472
35. G. Degrassi, P. Slavich, F. Zwirner, On the neutral Higgs boson masses in the MSSM for arbitrary stop mixing. Nucl. Phys. B **611**, 403–422 (2001). arXiv:hep-ph/0105096
36. A. Brignole, G. Degrassi, P. Slavich, F. Zwirner, On the $\mathcal{O}(\alpha_t^2)$ two loop corrections to the neutral Higgs boson masses in the MSSM. Nucl. Phys. B **631**, 195–218 (2002). arXiv:hep-ph/0112177
37. A. Brignole, G. Degrassi, P. Slavich, F. Zwirner, On the two loop sbottom corrections to the neutral Higgs boson masses in the MSSM. Nucl. Phys. B **643**, 79–92 (2002). arXiv:hep-ph/0206101
38. A. Dedes, G. Degrassi, P. Slavich, On the two loop Yukawa corrections to the MSSM Higgs boson masses at large tan beta. Nucl. Phys. B **672**, 144–162 (2003). arXiv:hep-ph/0305127
39. ATLAS Collaboration, M. Aaboud et al., Search for dark matter and other new phenomena in events with an energetic jet and large missing transverse momentum using the ATLAS detector. JHEP **01**, 126 (2018). arXiv:1711.03301 [hep-ex]
40. CMS Collaboration, A.M. Sirunyan et al., Search for the pair production of third-generation squarks with two-body decays to a bottom or charm quark and a neutralino in proton-proton collisions at $\sqrt{s}$ = 13 TeV. Phys. Lett. B **778**, 263–291 (2018). arXiv:1707.07274 [hep-ex]
41. G. Degrassi, S. Heinemeyer, W. Hollik, P. Slavich, G. Weiglein, Towards high precision predictions for the MSSM Higgs sector. Eur. Phys. J. C **28**, 133–143 (2003). arXiv:hep-ph/0212020
42. B.C. Allanach, A. Djouadi, J.L. Kneur, W. Porod, P. Slavich, Precise determination of the neutral Higgs boson masses in the MSSM. JHEP **09**, 044 (2004). arXiv:hep-ph/0406166
43. DELPHI, OPAL, ALEPH, LEP Working group for Higgs boson searches, L3 Collaboration, S. Schael et al., Search for neutral MSSM Higgs bosons at LEP. Eur. Phys. J. C **47**, 547–587 (2006). arXiv:hep-ex/0602042 [hep-ex]
44. J.S. Lee, A. Pilaftsis, M. Carena, S.Y. Choi, M. Drees, J.R. Ellis, C.E.M. Wagner, CPsuperH: a computational tool for Higgs phenomenology in the minimal supersymmetric standard model with explicit CP violation. Comput. Phys. Commun. **156**, 283–317 (2004). arXiv:hep-ph/0307377
45. J.S. Lee, M. Carena, J. Ellis, A. Pilaftsis, C.E.M. Wagner, CPsuperH2.0: an improved computational tool for Higgs phenomenology in the MSSM with explicit CP violation. Comput. Phys. Commun. **180**, 312–331 (2009). arXiv:0712.2360 [hep-ph]
46. J.S. Lee, M. Carena, J. Ellis, A. Pilaftsis, C.E.M. Wagner, CPsuperH2.3: an updated tool for phenomenology in the MSSM with explicit CP violation. Comput. Phys. Commun. **184**, 1220–1233 (2013). arXiv:1208.2212 [hep-ph]
47. A. Pilaftsis, C.E.M. Wagner, Higgs bosons in the minimal supersymmetric standard model with explicit CP violation. Nucl. Phys. B **553**, 3–42 (1999). arXiv:hep-ph/9902371
48. S.Y. Choi, M. Drees, J.S. Lee, Loop corrections to the neutral Higgs boson sector of the MSSM with explicit CP violation. Phys. Lett. B **481**, 57–66 (2000). arXiv:hep-ph/0002287
49. M. Carena, J.R. Ellis, A. Pilaftsis, C.E.M. Wagner, Renormalization group improved effective potential for the MSSM Higgs sec-

tor with explicit CP violation. Nucl. Phys. B **586**, 92–140 (2000). arXiv:hep-ph/0003180
50. C.A. Baker et al., An Improved experimental limit on the electric dipole moment of the neutron. Phys. Rev. Lett. **97**, 131801 (2006). arXiv:hep-ex/0602020
51. ACME Collaboration, J. Baron et al., Order of Magnitude smaller limit on the electric dipole moment of the electron. Science **343**, 269–272 (2014). arXiv:1310.7534 [physics.atom-ph]
52. S. Heinemeyer, W. Hollik, H. Rzehak, G. Weiglein, The Higgs sector of the complex MSSM at two-loop order: QCD contributions. Phys. Lett. B **652**, 300–309 (2007). arXiv:0705.0746 [hep-ph]
53. W. Hollik, S. Paßehr, Two-loop top-Yukawa-coupling corrections to the Higgs boson masses in the complex MSSM. Phys. Lett. B **733**, 144–150 (2014). arXiv:1401.8275 [hep-ph]
54. W. Hollik, S. Paßehr, Higgs boson masses and mixings in the complex MSSM with two-loop top-Yukawa-coupling corrections. JHEP **10**, 171 (2014). arXiv:1409.1687 [hep-ph]
55. W. Hollik, S. Paßehr, Two-loop top-Yukawa-coupling corrections to the charged Higgs-boson mass in the MSSM. Eur. Phys. J. C **75**(7), 336 (2015). arXiv:1502.02394 [hep-ph]
56. S. Paßehr, G. Weiglein, Two-loop top and bottom Yukawa corrections to the Higgs-boson masses in the complex MSSM. Eur. Phys. J. C **78**(3), 222 (2018). arXiv:1705.07909 [hep-ph]
57. S. Borowka, S. Paßehr, G. Weiglein, Complete two-loop QCD contributions to the lightest Higgs-boson mass in the MSSM with complex parameters. Eur. Phys. J. C **78**(7), 576 (2018). arXiv:1802.09886 [hep-ph]
58. S. Liebler, S. Patel, G. Weiglein, Phenomenology of on-shell Higgs production in the MSSM with complex parameters. Eur. Phys. J. C **77**(5), 305 (2017). arXiv:1611.09308 [hep-ph]
59. E. Fuchs, S. Thewes, G. Weiglein, Interference effects in BSM processes with a generalised narrow-width approximation. Eur. Phys. J. C **75**, 254 (2015). arXiv:1411.4652 [hep-ph]
60. E. Fuchs, G. Weiglein, Breit–Wigner approximation for propagators of mixed unstable states. JHEP **09**, 079 (2017). arXiv:1610.06193 [hep-ph]
61. E. Fuchs, G. Weiglein, Impact of CP-violating interference effects on MSSM Higgs searches. Eur. Phys. J. C **78**(2), 87 (2018). arXiv:1705.05757 [hep-ph]
62. E. Bagnaschi et al., Benchmark scenarios for low $\tan\beta$ in the MSSM. LHCHXSWG-2015-002 (2015)
63. G. Lee, C.E.M. Wagner, Higgs bosons in heavy supersymmetry with an intermediate m_A. Phys. Rev. D **92**(7), 075032 (2015). arXiv:1508.00576 [hep-ph]
64. E. Bagnaschi, F. Brümmer, W. Buchmüller, A. Voigt, G. Weiglein, Vacuum stability and supersymmetry at high scales with two Higgs doublets. JHEP **03**, 158 (2016). arXiv:1512.07761 [hep-ph]
65. H. Bahl, W. Hollik, Precise prediction of the MSSM Higgs boson masses for low M_A. JHEP **07**, 182 (2018). arXiv:1805.00867 [hep-ph]
66. A. Djouadi, J. Quevillon, The MSSM Higgs sector at a high M_{SUSY}: reopening the low $\tan\beta$ regime and heavy Higgs searches. JHEP **10**, 028 (2013). arXiv:1304.1787 [hep-ph]
67. L. Maiani, A.D. Polosa, V. Riquer, Bounds to the Higgs sector masses in minimal supersymmetry from LHC data. Phys. Lett. B **724**, 274–277 (2013). arXiv:1305.2172 [hep-ph]
68. A. Djouadi, L. Maiani, G. Moreau, A. Polosa, J. Quevillon, V. Riquer, The post-Higgs MSSM scenario: Habemus MSSM? Eur. Phys. J. C **73**, 2650 (2013). arXiv:1307.5205 [hep-ph]
69. A. Djouadi, L. Maiani, A. Polosa, J. Quevillon, V. Riquer, Fully covering the MSSM Higgs sector at the LHC. JHEP **06**, 168 (2015). arXiv:1502.05653 [hep-ph]
70. J.F. Gunion, H.E. Haber, The CP conserving two Higgs doublet model: the approach to the decoupling limit. Phys. Rev. D **67**, 075019 (2003). arXiv:hep-ph/0207010
71. N. Craig, J. Galloway, S. Thomas, Searching for signs of the second Higgs doublet (2013). arXiv:1305.2424 [hep-ph]
72. M. Carena, I. Low, N.R. Shah, C.E.M. Wagner, Impersonating the standard Model Higgs Boson: alignment without decoupling. JHEP **04**, 015 (2014). arXiv:1310.2248 [hep-ph]
73. M. Carena, H.E. Haber, I. Low, N.R. Shah, C.E.M. Wagner, Complementarity between nonstandard Higgs Boson searches and precision Higgs Boson measurements in the MSSM. Phys. Rev. D **91**(3), 035003 (2015). arXiv:1410.4969 [hep-ph]
74. R.V. Harlander, S. Liebler, H. Mantler, SusHi: a program for the calculation of Higgs production in gluon fusion and bottom-quark annihilation in the standard model and the MSSM. Comput. Phys. Commun. **184**, 1605–1617 (2013). arXiv:1212.3249 [hep-ph]
75. R.V. Harlander, S. Liebler, H. Mantler, SusHi Bento: beyond NNLO and the heavy-top limit. Comput. Phys. Commun. **212**, 239–257 (2017). arXiv:1605.03190 [hep-ph]
76. P. Bechtle, O. Brein, S. Heinemeyer, G. Weiglein, K.E. Williams, HiggsBounds: confronting arbitrary Higgs sectors with exclusion bounds from LEP and the Tevatron. Comput. Phys. Commun. **181**, 138–167 (2010). arXiv:0811.4169 [hep-ph]
77. P. Bechtle, O. Brein, S. Heinemeyer, G. Weiglein, K.E. Williams, HiggsBounds 2.0.0: confronting neutral and charged Higgs sector predictions with exclusion bounds from LEP and the Tevatron. Comput. Phys. Commun. **182**, 2605–2631 (2011). arXiv:1102.1898 [hep-ph]
78. P. Bechtle, O. Brein, S. Heinemeyer, O. Stål, T. Stefaniak, G. Weiglein, K.E. Williams, $HiggsBounds - 4$: improved tests of extended Higgs sectors against exclusion bounds from LEP, the Tevatron and the LHC. Eur. Phys. J. C **74**(3), 2693 (2014). arXiv:1311.0055 [hep-ph]
79. P. Bechtle, S. Heinemeyer, O. Stål, T. Stefaniak, G. Weiglein, Applying exclusion likelihoods from LHC searches to extended Higgs sectors. Eur. Phys. J. C **75**(9), 421 (2015). arXiv:1507.06706 [hep-ph]
80. P. Bechtle, S. Heinemeyer, O. Stål, T. Stefaniak, G. Weiglein, $HiggsSignals$: confronting arbitrary Higgs sectors with measurements at the Tevatron and the LHC. Eur. Phys. J. C **74**(2), 2711 (2014). arXiv:1305.1933 [hep-ph]
81. http://www.feynhiggs.de/cgi-bin/fhman.cgi?man=FHSetFlags
82. A. Denner, S. Heinemeyer, I. Puljak, D. Rebuzzi, M. Spira, Standard model Higgs-Boson branching ratios with uncertainties. Eur. Phys. J. C **71**, 1753 (2011). arXiv:1107.5909 [hep-ph]
83. A. Dabelstein, Fermionic decays of neutral MSSM Higgs Bosons at the one loop level. Nucl. Phys. B **456**, 25–56 (1995). arXiv:hep-ph/9503443
84. S. Heinemeyer, W. Hollik, J. Rosiek, G. Weiglein, Neutral MSSM Higgs boson production at e+ e- colliders in the Feynman diagrammatic approach. Eur. Phys. J. C **19**, 535–546 (2001). arXiv:hep-ph/0102081
85. K.E. Williams, G. Weiglein, Precise predictions for $h_a \to h_b h_c$ decays in the complex MSSM. Phys. Lett. B **660**, 217–227 (2008). arXiv:0710.5320 [hep-ph]
86. K.E. Williams, H. Rzehak, G. Weiglein, Higher order corrections to Higgs boson decays in the MSSM with complex parameters. Eur. Phys. J. C **71**, 1669 (2011). arXiv:1103.1335 [hep-ph]
87. T. Banks, Supersymmetry and the quark mass matrix. Nucl. Phys. B **303**, 172–188 (1988)
88. L.J. Hall, R. Rattazzi, U. Sarid, The top quark mass in supersymmetric SO(10) unification. Phys. Rev. D **50**, 7048–7065 (1994). arXiv:hep-ph/9306309
89. R. Hempfling, Yukawa coupling unification with supersymmetric threshold corrections. Phys. Rev. D **49**, 6168–6172 (1994)
90. M. Carena, M. Olechowski, S. Pokorski, C.E.M. Wagner, Electroweak symmetry breaking and bottom–top Yukawa unification. Nucl. Phys. B **426**, 269–300 (1994). arXiv:hep-ph/9402253

91. M. Carena, D. Garcia, U. Nierste, C.E.M. Wagner, Effective Lagrangian for the $\bar{t}bH^+$ interaction in the MSSM and charged Higgs phenomenology. Nucl. Phys. B **577**, 88–120 (2000). arXiv:hep-ph/9912516
92. M. Carena, D. Garcia, U. Nierste, C.E.M. Wagner, $b \to s\gamma$ and supersymmetry with large tan β. Phys. Lett. B **499**, 141–146 (2001). arXiv:hep-ph/0010003
93. L. Hofer, U. Nierste, D. Scherer, Resummation of tan–beta-enhanced supersymmetric loop corrections beyond the decoupling limit. JHEP **10**, 081 (2009). arXiv:0907.5408 [hep-ph]
94. A. Bredenstein, A. Denner, S. Dittmaier, M.M. Weber, Precise predictions for the Higgs-Boson decay H $\to$ WW/ZZ $\to$ 4 leptons. Phys. Rev. D **74**, 013004 (2006). arXiv:hep-ph/0604011
95. A. Bredenstein, A. Denner, S. Dittmaier, M.M. Weber, Radiative corrections to the semileptonic and hadronic Higgs-boson decays H $\to$ W W / Z Z $\to$ 4 fermions. JHEP **02**, 080 (2007). arXiv:hep-ph/0611234
96. M. Spira, A. Djouadi, D. Graudenz, P.M. Zerwas, Higgs boson production at the LHC. Nucl. Phys. B **453**, 17–82 (1995). arXiv:hep-ph/9504378
97. R. Harlander, P. Kant, Higgs production and decay: analytic results at next-to-leading order QCD. JHEP **12**, 015 (2005). arXiv:hep-ph/0509189
98. R.V. Harlander, W.B. Kilgore, Next-to-next-to-leading order Higgs production at Hadron colliders. Phys. Rev. Lett. **88**, 201801 (2002). arXiv:hep-ph/0201206
99. C. Anastasiou, K. Melnikov, Higgs Boson production at Hadron colliders in NNLO QCD. Nucl. Phys. B **646**, 220–256 (2002). arXiv:hep-ph/0207004
100. V. Ravindran, J. Smith, W.L. van Neerven, NNLO corrections to the total cross-section for Higgs boson production in hadron–hadron collisions. Nucl. Phys. B **665**, 325–366 (2003). arXiv:hep-ph/0302135
101. R.V. Harlander, W.B. Kilgore, Production of a pseudoscalar Higgs boson at hadron colliders at next-to-next-to leading order. JHEP **10**, 017 (2002). arXiv:hep-ph/0208096
102. C. Anastasiou, K. Melnikov, Pseudoscalar Higgs boson production at hadron colliders in NNLO QCD. Phys. Rev. D **67**, 037501 (2003). arXiv:hep-ph/0208115
103. C. Anastasiou, C. Duhr, F. Dulat, E. Furlan, T. Gehrmann, F. Herzog, B. Mistlberger, Higgs Boson gluon-fusion production beyond threshold in N^{3}LO QCD. JHEP **03**, 091 (2015). arXiv:1411.3584 [hep-ph]
104. C. Anastasiou, C. Duhr, F. Dulat, E. Furlan, F. Herzog, B. Mistlberger, Soft expansion of double-real-virtual corrections to Higgs production at N^{3}LO. JHEP **08**, 051 (2015). arXiv:1505.04110 [hep-ph]
105. C. Anastasiou, C. Duhr, F. Dulat, E. Furlan, T. Gehrmann, F. Herzog, A. Lazopoulos, B. Mistlberger, High precision determination of the gluon fusion Higgs Boson cross-section at the LHC. JHEP **05**, 058 (2016). arXiv:1602.00695 [hep-ph]
106. B. Mistlberger, Higgs Boson production at hadron colliders at N^{3}LO in QCD. JHEP **05**, 028 (2018). arXiv:1802.00833 [hep-ph]
107. G. Degrassi, P. Slavich, NLO QCD bottom corrections to Higgs boson production in the MSSM. JHEP **11**, 044 (2010). arXiv:1007.3465 [hep-ph]
108. G. Degrassi, S. Di Vita, P. Slavich, NLO QCD corrections to pseudoscalar Higgs production in the MSSM. JHEP **08**, 128 (2011). arXiv:1107.0914 [hep-ph]
109. G. Degrassi, S. Di Vita, P. Slavich, On the NLO QCD corrections to the production of the heaviest neutral Higgs scalar in the MSSM. Eur. Phys. J. C **72**, 2032 (2012). arXiv:1204.1016 [hep-ph]
110. U. Aglietti, R. Bonciani, G. Degrassi, A. Vicini, Two loop light fermion contribution to Higgs production and decays. Phys. Lett. B **595**, 432–441 (2004). arXiv:hep-ph/0404071
111. R. Bonciani, G. Degrassi, A. Vicini, On the generalized harmonic polylogarithms of one complex variable. Comput. Phys. Commun. **182**, 1253–1264 (2011). arXiv:1007.1891 [hep-ph]
112. J. Butterworth et al., PDF4LHC recommendations for LHC run II. J. Phys. G **43**, 023001 (2016). arXiv:1510.03865 [hep-ph]
113. R. Harlander, M. Krämer, M. Schumacher, Bottom-quark associated Higgs-Boson production: reconciling the four- and five-flavour scheme approach (2011). arXiv:1112.3478 [hep-ph]
114. R.V. Harlander, W.B. Kilgore, Higgs Boson production in bottom quark fusion at next-to-next-to leading order. Phys. Rev. D **68**, 013001 (2003). arXiv:hep-ph/0304035
115. S. Dittmaier, M. Krämer, M. Spira, Higgs radiation off bottom quarks at the Tevatron and the CERN LHC. Phys. Rev. D **70**, 074010 (2004). arXiv:hep-ph/0309204
116. S. Dawson, C.B. Jackson, L. Reina, D. Wackeroth, Exclusive Higgs Boson production with bottom quarks at hadron colliders. Phys. Rev. D **69**, 074027 (2004). arXiv:hep-ph/0311067
117. M. Wiesemann, R. Frederix, S. Frixione, V. Hirschi, F. Maltoni, P. Torrielli, Higgs production in association with bottom quarks. JHEP **02**, 132 (2015). arXiv:1409.5301 [hep-ph]
118. M. Bonvini, A.S. Papanastasiou, F.J. Tackmann, Resummation and matching of b-quark mass effects in $b\bar{b}H$ production. JHEP **11**, 196 (2015). arXiv:1508.03288 [hep-ph]
119. M. Bonvini, A.S. Papanastasiou, F.J. Tackmann, Matched predictions for the $b\bar{b}H$ cross section at the 13 TeV LHC. JHEP **10**, 053 (2016). arXiv:1605.01733 [hep-ph]
120. S. Forte, D. Napoletano, M. Ubiali, Higgs production in bottom-quark fusion in a matched scheme. Phys. Lett. B **751**, 331–337 (2015). arXiv:1508.01529 [hep-ph]
121. S. Forte, D. Napoletano, M. Ubiali, Higgs production in bottom-quark fusion: matching beyond leading order. Phys. Lett. B **763**, 190–196 (2016). arXiv:1607.00389 [hep-ph]
122. E. Bagnaschi, R.V. Harlander, S. Liebler, H. Mantler, P. Slavich, A. Vicini, Towards precise predictions for Higgs-boson production in the MSSM. JHEP **06**, 167 (2014). arXiv:1404.0327 [hep-ph]
123. E.L. Berger, T. Han, J. Jiang, T. Plehn, Associated production of a top quark and a charged Higgs Boson. Phys. Rev. D **71**, 115012 (2005). arXiv:hep-ph/0312286
124. S. Dittmaier, M. Krämer, M. Spira, M. Walser, Charged-Higgs-Boson production at the LHC: NLO supersymmetric QCD corrections. Phys. Rev. D **83**, 055005 (2011). arXiv:0906.2648 [hep-ph]
125. M. Flechl, R. Klees, M. Krämer, M. Spira, M. Ubiali, Improved cross-section predictions for heavy charged Higgs boson production at the LHC. Phys. Rev. D **91**(7), 075015 (2015). arXiv:1409.5615 [hep-ph]
126. C. Degrande, M. Ubiali, M. Wiesemann, M. Zaro, Heavy charged Higgs boson production at the LHC. JHEP **10**, 145 (2015). arXiv:1507.02549 [hep-ph]
127. C. Degrande, R. Frederix, V. Hirschi, M. Ubiali, M. Wiesemann, M. Zaro, Accurate predictions for charged Higgs production: closing the $m_{H^\pm} \sim m_t$ window. Phys. Lett. B **772**, 87–92 (2017). arXiv:1607.05291 [hep-ph]
128. A.H. Hoang, I.W. Stewart, Top mass measurements from jets and the Tevatron Top-Quark Mass. Nucl. Phys. Proc. Suppl. **185**, 220–226 (2008). arXiv:0808.0222 [hep-ph]
129. M. Butenschoen, B. Dehnadi, A.H. Hoang, V. Mateu, M. Preisser, I.W. Stewart, Top quark mass calibration for Monte Carlo event generators. Phys. Rev. Lett. **117**(23), 232001 (2016). arXiv:1608.01318 [hep-ph]
130. P. Nason, The top mass in hadronic collisions (2017). arXiv:1712.02796 [hep-ph]
131. Particle Data Group Collaboration, C. Patrignani et al., Review of particle physics. Chin. Phys. C **40**(10), 100001 (2016)
132. ATLAS Collaboration, M. Aaboud et al., Search for squarks and gluinos in events with an isolated lepton, jets, and missing trans-

verse momentum at $\sqrt{s} = 13$ TeV with the ATLAS detector. Phys. Rev. D **96**(11), 112010 (2017). arXiv:1708.08232 [hep-ex]
133. ATLAS Collaboration, M. Aaboud et al., Search for squarks and gluinos in final states with jets and missing transverse momentum using 36 fb^{-1} of $\sqrt{s}$=13 TeV pp collision data with the ATLAS detector. Phys. Rev. D **97**(11), 112001 (2018). arXiv:1712.02332 [hep-ex]
134. CMS Collaboration, A.M. Sirunyan et al., Search for supersymmetry in multijet events with missing transverse momentum in proton-proton collisions at 13 TeV. Phys. Rev. D **96**(3), 032003 (2017). arXiv:1704.07781 [hep-ex]
135. CMS Collaboration, A.M. Sirunyan et al., Search for new phenomena with the M_{T2} variable in the all-hadronic final state produced in proton-proton collisions at $\sqrt{s} = 13$ TeV. Eur. Phys. J. C **77**(10), 710 (2017). arXiv:1705.04650 [hep-ex]
136. CMS Collaboration, A.M. Sirunyan et al., Search for natural and split supersymmetry in proton-proton collisions at $\sqrt{s} = 13$ TeV in final states with jets and missing transverse momentum. JHEP **05**, 025 (2018). arXiv:1802.02110 [hep-ex]
137. ATLAS Collaboration, M. Aaboud et al., Search for additional heavy neutral Higgs and gauge Bosons in the ditau final state produced in 36 fb^{-1} of pp collisions at $\sqrt{s} = 13$ TeV with the ATLAS detector. JHEP **01**, 055 (2018). arXiv:1709.07242 [hep-ex]
138. CMS Collaboration, A.M. Sirunyan et al., Search for additional neutral MSSM Higgs bosons in the $\tau\tau$ final state in proton-proton collisions at $\sqrt{s} = 13$ TeV. JHEP **09**, 007 (2018). arXiv:1803.06553 [hep-ex]
139. CMS Collaboration, Search for additional neutral Higgs bosons decaying to a pair of tau leptons in pp collisions at $\sqrt{s} = 7$ and 8 TeV. CMS-PAS-HIG-14-029 (2015)
140. ATLAS Collaboration, G. Aad et al., Search for an additional, heavy Higgs boson in the $H \to ZZ$ decay channel at $\sqrt{s} = 8$ TeV in pp collision data with the ATLAS detector. Eur. Phys. J. C **76**(1), 45 (2016). arXiv:1507.05930 [hep-ex]
141. ATLAS Collaboration, M. Aaboud et al., Search for heavy ZZ resonances in the $\ell^+\ell^-\ell^+\ell^-$ and $\ell^+\ell^-\nu\bar{\nu}$ final states using proton-proton collisions at $\sqrt{s} = 13$ TeV with the ATLAS detector. Eur. Phys. J. C **78**(4), 293 (2018). arXiv:1712.06386 [hep-ex]
142. CMS Collaboration, V. Khachatryan et al., Search for a Higgs boson in the mass range from 145 to 1000 GeV decaying to a pair of W or Z bosons. JHEP **10**, 144 (2015). arXiv:1504.00936 [hep-ex]
143. CMS Collaboration, A.M. Sirunyan et al., Search for a new scalar resonance decaying to a pair of Z bosons in proton-proton collisions at $\sqrt{s} = 13$ TeV. JHEP **06**, 127 (2018). arXiv:1804.01939 [hep-ex]
144. ATLAS Collaboration, G. Aad et al., Searches for Higgs boson pair production in the $hh \to bb\tau\tau, \gamma\gamma WW^*, \gamma\gamma bb, bbbb$ channels with the ATLAS detector. Phys. Rev. D **92**, 092004 (2015). arXiv:1509.04670 [hep-ex]
145. CMS Collaboration, A.M. Sirunyan et al., Search for Higgs boson pair production in events with two bottom quarks and two tau leptons in proton-proton collisions at $\sqrt{s}$ =13 TeV. Phys. Lett. B **778**, 101–127 (2018). arXiv:1707.02909 [hep-ex]
146. CMS Collaboration, A.M. Sirunyan et al., Search for resonant and nonresonant Higgs Boson pair production in the $b\bar{b}\ell\nu\ell\nu$ final state in proton-proton collisions at $\sqrt{s} = 13$ TeV. JHEP **01**, 054 (2018). arXiv:1708.04188 [hep-ex]
147. ATLAS Collaboration, G. Aad et al., Search for new phenomena in events with at least three photons collected in pp collisions at $\sqrt{s} = 8$ TeV with the ATLAS detector. Eur. Phys. J. C **76**(4), 210 (2016). arXiv:1509.05051 [hep-ex]
148. CMS Collaboration, V. Khachatryan et al., Search for light bosons in decays of the 125 GeV Higgs boson in proton–proton collisions at $\sqrt{s} = 8$ TeV. JHEP **10**, 076 (2017). arXiv:1701.02032 [hep-ex]
149. ATLAS Collaboration, G. Aad et al., Search for a CP-odd Higgs boson decaying to Zh in pp collisions at $\sqrt{s} = 8$ TeV with the ATLAS detector. Phys. Lett. B **744**, 163–183 (2015). arXiv:1502.04478 [hep-ex]
150. CMS Collaboration, V. Khachatryan et al., Search for a pseudoscalar boson decaying into a Z boson and the 125 GeV Higgs boson in $\ell^+\ell^- b\bar{b}$ final states. Phys. Lett. B **748**, 221–243 (2015). arXiv:1504.04710 [hep-ex]
151. CMS Collaboration, V. Khachatryan et al., Search for a charged Higgs Boson in pp collisions at $\sqrt{s} = 8$ TeV. JHEP **11**, 018 (2015). arXiv:1508.07774 [hep-ex]
152. CMS Collaboration, Search for charged Higgs bosons with the $H^\pm \to \tau^\pm\nu_\tau$ decay channel in the fully hadronic final state at $\sqrt{s} = 13$ TeV. CMS-PAS-HIG-16-031 (2016)
153. ATLAS Collaboration, G. Aad et al., Search for charged Higgs bosons decaying via $H^\pm \to \tau^\pm\nu$ in fully hadronic final states using pp collision data at $\sqrt{s} = 8$ TeV with the ATLAS detector. JHEP **03**, 088 (2015). arXiv:1412.6663 [hep-ex]
154. ATLAS Collaboration, M. Aaboud et al., Search for charged Higgs bosons decaying via $H^\pm \to \tau^\pm\nu_\tau$ in the τ+jets and τ+lepton final states with 36 fb^{-1} of pp collision data recorded at $\sqrt{s} = 13$ TeV with the ATLAS experiment. JHEP **09**, 139 (2018). arXiv:1807.07915 [hep-ex]
155. ATLAS Collaboration, G. Aad et al., Search for charged Higgs bosons in the $H^\pm \to tb$ decay channel in pp collisions at $\sqrt{s} = 8$ TeV using the ATLAS detector. JHEP **03**, 127 (2016). arXiv:1512.03704 [hep-ex]
156. ATLAS Collaboration, Search for charged Higgs bosons in the $H^\pm \to tb$ decay channel in pp collisions at $\sqrt{s} = 13$ TeV using the ATLAS detector. ATLAS-CONF-2016-089 (2016)
157. ATLAS Collaboration, Measurements of the Higgs boson production cross section via Vector Boson Fusion and associated WH production in the $WW^* \to \ell\nu\ell\nu$ decay mode with the ATLAS detector at $\sqrt{s}$ = 13 TeV. ATLAS-CONF-2016-112 (2016)
158. ATLAS Collaboration, Measurement of gluon fusion and vector boson fusion Higgs boson production cross-sections in the $H \to WW^* \to e\nu\mu\nu$ decay channel in pp collisions at $\sqrt{s} = 13$ TeV with the ATLAS detector. ATLAS-CONF-2018-004 (2018)
159. ATLAS Collaboration, M. Aaboud et al., Evidence for the $H \to b\bar{b}$ decay with the ATLAS detector. JHEP **12**, 024 (2017). arXiv:1708.03299 [hep-ex]
160. ATLAS Collaboration, M. Aaboud et al., Measurement of the Higgs Boson coupling properties in the $H \to ZZ^* \to 4\ell$ decay channel at $\sqrt{s}$ = 13 TeV with the ATLAS detector. JHEP **03**, 095 (2018). arXiv:1712.02304 [hep-ex]
161. ATLAS Collaboration, M. Aaboud et al., Evidence for the associated production of the Higgs boson and a top quark pair with the ATLAS detector. Phys. Rev. D **97**(7), 072003 (2018). arXiv:1712.08891 [hep-ex]
162. ATLAS Collaboration, M. Aaboud et al., Search for the standard model Higgs Boson produced in association with top quarks and decaying into a $b\bar{b}$ pair in pp collisions at $\sqrt{s}$ = 13 TeV with the ATLAS detector. Phys. Rev. D **97**(7), 072016 (2018). arXiv:1712.08895 [hep-ex]
163. ATLAS Collaboration, M. Aaboud et al., Measurements of Higgs boson properties in the diphoton decay channel with 36 fb^{-1} of pp collision data at $\sqrt{s} = 13$ TeV with the ATLAS detector. Phys. Rev. D **98**, 052005 (2018). arXiv:1802.04146 [hep-ex]
164. CMS Collaboration, Measurements of properties of the Higgs boson in the diphoton decay channel with the full 2016 data set. CMS-PAS-HIG-16-040 (2017)
165. CMS Collaboration, A.M. Sirunyan et al., Measurements of properties of the Higgs Boson decaying into the four-lepton final state in pp collisions at $\sqrt{s} = 13$ TeV. JHEP **11**, 047 (2017). arXiv:1706.09936 [hep-ex]

166. CMS Collaboration, A.M. Sirunyan et al., Observation of the Higgs boson decay to a pair of τ leptons with the CMS detector. Phys. Lett. B **779**, 283–316 (2018). arXiv:1708.00373 [hep-ex]
167. CMS Collaboration, A.M. Sirunyan et al., Inclusive search for a highly boosted Higgs Boson decaying to a bottom quark-antiquark pair. Phys. Rev. Lett. **120**(7), 071802 (2018). arXiv:1709.05543 [hep-ex]
168. CMS Collaboration, A.M. Sirunyan et al., Evidence for the Higgs Boson decay to a bottom quark-antiquark pair. Phys. Lett. B **780**, 501–532 (2018). arXiv:1709.07497 [hep-ex]
169. CMS Collaboration, A.M. Sirunyan et al., Evidence for associated production of a Higgs Boson with a top quark pair in final states with electrons, muons, and hadronically decaying τ leptons at $\sqrt{s} = 13$ TeV. JHEP **08**, 066 (2018). arXiv:1803.05485 [hep-ex]
170. CMS Collaboration, A.M. Sirunyan et al., Search for $t\bar{t}H$ production in the all-jet final state in proton-proton collisions at $\sqrt{s} =$ 13 TeV. JHEP **06**, 101 (2018). arXiv:1803.06986 [hep-ex]
171. CMS Collaboration, A.M. Sirunyan et al., Search for $t\bar{t}H$productionintheH $\rightarrow b\bar{b}$ decay channel with leptonic $t\bar{t}$ decays in proton–proton collisions at $\sqrt{s} = 13$ TeV (2018). arXiv:1804.03682 [hep-ex]
172. CMS Collaboration, A.M. Sirunyan et al., Measurements of properties of the Higgs Boson decaying to a W boson pair in pp collisions at $\sqrt{s} = 13TeV$. Phys. Lett. **B 791**, 96 (2019). arXiv:1806.05246 [hep-ex]
173. CMS Collaboration, A.M. Sirunyan et al., Search for the Higgs Boson decaying to two muons in proton-proton collisions at $\sqrt{s} = 13TeV$. Phys. Rev. Lett. **122**(2), 021801 (2019). arXiv:1807.06325 [hep-ex]
174. ATLAS Collaboration, M. Aaboud et al., Search for direct top squark pair production in final states with two leptons in $\sqrt{s} =$ 13 TeV pp collisions with the ATLAS detector. Eur. Phys. J. C **77**(12), 898 (2017). arXiv:1708.03247 [hep-ex]
175. ATLAS Collaboration, M. Aaboud et al., Search for a scalar partner of the top quark in the jets plus missing transverse momentum final state at $\sqrt{s}$=13 TeV with the ATLAS detector. JHEP **12**, 085 (2017). arXiv:1709.04183 [hep-ex]
176. ATLAS Collaboration, M. Aaboud et al., Search for top-squark pair production in final states with one lepton, jets, and missing transverse momentum using 36 fb^{-1} of $\sqrt{s} = 13$ TeV pp collision data with the ATLAS detector. JHEP **06**, 108 (2018). arXiv:1711.11520 [hep-ex]
177. CMS Collaboration, A.M. Sirunyan et al., Search for top squark pair production in pp collisions at $\sqrt{s} = 13$ TeV using single lepton events. JHEP **10**, 019 (2017). arXiv:1706.04402 [hep-ex]
178. CMS Collaboration, A.M. Sirunyan et al., Search for direct production of supersymmetric partners of the top quark in the all-jets final state in proton-proton collisions at $\sqrt{s} = 13$ TeV. JHEP **10**, 005 (2017). arXiv:1707.03316 [hep-ex]
179. CMS Collaboration, A.M. Sirunyan et al., Search for top squarks and dark matter particles in opposite-charge dilepton final states at $\sqrt{s} = 13$ TeV. Phys. Rev. D **97**(3), 032009 (2018). arXiv:1711.00752 [hep-ex]
180. ATLAS Collaboration, M. Aaboud et al., Search for supersymmetry in final states with two same-sign or three leptons and jets using 36 fb^{-1} of $\sqrt{s} = 13$ TeV pp collision data with the ATLAS detector. JHEP **09**, 084 (2017). arXiv:1706.03731 [hep-ex]
181. ATLAS Collaboration, M. Aaboud et al., Search for supersymmetry in events with b-tagged jets and missing transverse momentum in pp collisions at $\sqrt{s} = 13$ TeV with the ATLAS detector. JHEP **11**, 195 (2017). arXiv:1708.09266 [hep-ex]
182. M. Carena, S. Gori, N.R. Shah, C.E.M. Wagner, A 125 GeV SM-like Higgs in the MSSM and the $\gamma\gamma$ rate. JHEP **03**, 014 (2012). arXiv:1112.3336 [hep-ph]
183. R. Benbrik, M. Gomez Bock, S. Heinemeyer, O. Stal, G. Weiglein, L. Zeune, Confronting the MSSM and the NMSSM with the discovery of a signal in the two photon channel at the LHC. Eur. Phys. J. C **72**, 2171 (2012). arXiv:1207.1096 [hep-ph]
184. M. Carena, S. Gori, N.R. Shah, C.E.M. Wagner, L.-T. Wang, Light stops, light staus and the 125 GeV Higgs. JHEP **08**, 087 (2013). arXiv:1303.4414 [hep-ph]
185. B. Batell, S. Jung, C.E.M. Wagner, Very light charginos and Higgs decays. JHEP **12**, 075 (2013). arXiv:1309.2297 [hep-ph]
186. A. Belyaev, S. Khalil, S. Moretti, M.C. Thomas, Light sfermion interplay in the 125 GeV MSSM Higgs production and decay at the LHC. JHEP **05**, 076 (2014). arXiv:1312.1935 [hep-ph]
187. S. Liebler, S. Profumo, T. Stefaniak, Light stop mass limits from Higgs rate measurements in the MSSM: Is MSSM electroweak baryogenesis still alive after all? JHEP **04**, 143 (2016). arXiv:1512.09172 [hep-ph]
188. J.R. Espinosa, I. Navarro, Radiative corrections to the Higgs boson mass for a hierarchical stop spectrum. Nucl. Phys. B **615**, 82–116 (2001). arXiv:hep-ph/0104047
189. M. Carena, G. Nardini, M. Quiros, C.E.M. Wagner, The effective theory of the light stop scenario. JHEP **10**, 062 (2008). arXiv:0806.4297 [hep-ph]
190. K.J. de Vries et al., The pMSSM10 after LHC Run 1. Eur. Phys. J. C **75**(9), 422 (2015). arXiv:1504.03260 [hep-ph]
191. LEPSUSYWG, ALEPH, DELPHI, L3 and OPAL experiments, Combined LEP Selectron/Smuon/Stau Results, 183-208 GeV LEPSUSYWG/04-01.1 (2019). http://lepsusy.web.cern.ch/lepsusy/www/sleptons_summer04/slep_final.html
192. LEPSUSYWG, ALEPH, DELPHI, L3 and OPAL experiments, Combined LEP Chargino Results, up to 208 GeV for large m0 LEPSUSYWG/01-03.1 (2019). http://lepsusy.web.cern.ch/lepsusy/www/inos_moriond01/charginos_pub.html
193. CMS Collaboration, A.M. Sirunyan et al., Search for supersymmetry in events with a τ lepton pair and missing transverse momentum in proton-proton collisions at $\sqrt{s} = 13$ TeV (2018). arXiv:1807.02048 [hep-ex]
194. A. Bharucha, S. Heinemeyer, F. von der Pahlen, Direct chargino-neutralino production at the LHC: interpreting the exclusion limits in the complex MSSM. Eur. Phys. J. C **73**(11), 2629 (2013). arXiv:1307.4237 [hep-ph]
195. ATLAS Collaboration, M. Aaboud et al., Search for the direct production of charginos and neutralinos in $\sqrt{s} = 13$ TeV pp collisions with the ATLAS detector. Eur. Phys. J. C **78**(2), 154 (2018). arXiv:1708.07875 [hep-ex]
196. ATLAS Collaboration, M. Aaboud et al., Search for electroweak production of supersymmetric particles in final states with two or three leptons at $\sqrt{s} = 13$ TeV with the ATLAS detector (2018). arXiv:1803.02762 [hep-ex]
197. ATLAS Collaboration, M. Aaboud et al., Search for chargino-neutralino production using recursive jigsaw reconstruction in final states with two or three charged leptons in proton-proton collisions at $\sqrt{s} = 13$ TeV with the ATLAS detector (2018). arXiv:1806.02293 [hep-ex]
198. CMS Collaboration, A.M. Sirunyan et al., Combined search for electroweak production of charginos and neutralinos in proton-proton collisions at $\sqrt{s} = 13$ TeV. JHEP **03**, 160 (2018). arXiv:1801.03957 [hep-ex]
199. H.P. Nilles, M. Srednicki, D. Wyler, Weak interaction breakdown induced by supergravity. Phys. Lett. B **120**, 346 (1983)
200. J.M. Frere, D.R.T. Jones, S. Raby, Fermion masses and induction of the weak scale by supergravity. Nucl. Phys. B **222**, 11–19 (1983)
201. L. Alvarez-Gaume, J. Polchinski, M.B. Wise, Minimal low-energy supergravity. Nucl. Phys. B **221**, 495 (1983)
202. J.P. Derendinger, C.A. Savoy, Quantum effects and SU(2) x U(1) breaking in supergravity gauge theories. Nucl. Phys. B **237**, 307–328 (1984)

203. M. Claudson, L.J. Hall, I. Hinchliffe, Low-energy supergravity: false vacua and vacuous predictions. Nucl. Phys. B **228**, 501–528 (1983)
204. C. Kounnas, A.B. Lahanas, D.V. Nanopoulos, M. Quiros, Low-energy behavior of realistic locally supersymmetric grand unified theories. Nucl. Phys. B **236**, 438–466 (1984)
205. J. Hisano, S. Sugiyama, Charge-breaking constraints on left-right mixing of stau's. Phys. Lett. B **696**, 92–96 (2011). arXiv:1011.0260 [hep-ph] [**Erratum: Phys. Lett. B 719, 472 (2013)**]
206. M. Carena, S. Gori, I. Low, N.R. Shah, C.E.M. Wagner, Vacuum stability and Higgs Diphoton decays in the MSSM. JHEP **02**, 114 (2013). arXiv:1211.6136 [hep-ph]
207. T. Kitahara, T. Yoshinaga, Stau with large mass difference and enhancement of the Higgs to Diphoton decay rate in the MSSM. JHEP **05**, 035 (2013). arXiv:1303.0461 [hep-ph]
208. J.E. Camargo-Molina, B. O'Leary, W. Porod, F. Staub, **Vevacious**: a tool for finding the global minima of one-loop effective potentials with many scalars. Eur. Phys. J C **73**(10), 2588 (2013). arXiv:1307.1477 [hep-ph]
209. J.E. Camargo-Molina, B. Garbrecht, B. O'Leary, W. Porod, F. Staub, Constraining the natural MSSM through tunneling to color-breaking vacua at zero and non-zero temperature. Phys. Lett. B **737**, 156–161 (2014). arXiv:1405.7376 [hep-ph]
210. C.L. Wainwright, CosmoTransitions: computing cosmological phase transition temperatures and bubble profiles with multiple fields. Comput. Phys. Commun. **183**, 2006–2013 (2012). arXiv:1109.4189 [hep-ph]
211. F. Staub, SARAH 4: a tool for (not only SUSY) model builders. Comput. Phys. Commun. **185**, 1773–1790 (2014). arXiv:1309.7223 [hep-ph]
212. CMS Collaboration, A.M. Sirunyan et al., Search for new physics in events with two soft oppositely charged leptons and missing transverse momentum in proton-proton collisions at $\sqrt{s} = 13$ TeV. Phys. Lett. B **782**, 440–467 (2018). arXiv:1801.01846 [hep-ex]
213. ATLAS Collaboration, M. Aaboud et al., Search for electroweak production of supersymmetric states in scenarios with compressed mass spectra at $\sqrt{s} = 13$ TeV with the ATLAS detector. Phys. Rev. D **97**(5), 052010 (2018). arXiv:1712.08119 [hep-ex]
214. M. Drees, H. Dreiner, D. Schmeier, J. Tattersall, J.S. Kim, CheckMATE: confronting your favourite New physics model with LHC data. Comput. Phys. Commun. **187**, 227–265 (2015). arXiv:1312.2591 [hep-ph]
215. D. Dercks, N. Desai, J.S. Kim, K. Rolbiecki, J. Tattersall, T. Weber, CheckMATE 2: from the model to the limit. Comput. Phys. Commun. **221**, 383–418 (2017). arXiv:1611.09856 [hep-ph]
216. DELPHES 3 Collaboration, J. de Favereau, C. Delaere, P. Demin, A. Giammanco, V. Lemaître, A. Mertens, M. Selvaggi, DELPHES 3, A modular framework for fast simulation of a generic collider experiment. JHEP **02**, 057 (2014). arXiv:1307.6346 [hep-ex]
217. M. Cacciari, G.P. Salam, G. Soyez, FastJet user manual. Eur. Phys. J. C **72**, 1896 (2012). arXiv:1111.6097 [hep-ph]
218. M. Cacciari, G.P. Salam, Dispelling the N^3 myth for the k_t jet-finder. Phys. Lett. B **641**, 57–61 (2006). arXiv:hep-ph/0512210
219. M. Cacciari, G.P. Salam, G. Soyez, The anti-k_t jet clustering algorithm. JHEP **04**, 063 (2008). arXiv:0802.1189 [hep-ph]
220. A.L. Read, Presentation of search results: the CL(s) technique. J. Phys. G **28**, 2693–2704 (2002)
221. M. Muhlleitner, A. Djouadi, Y. Mambrini, SDECAY: A Fortran code for the decays of the supersymmetric particles in the MSSM. Comput. Phys. Commun. **168**, 46–70 (2005). arXiv:hep-ph/0311167
222. CMS Collaboration, Search for new physics in the compressed mass spectra scenario using events with two soft opposite-sign leptons and missing momentum energy at 13 TeV. CMS-PAS-SUS-16-025 (2016)
223. CMS Collaboration, A.M. Sirunyan et al., Search for electroweak production of charginos and neutralinos in multilepton final states in proton-proton collisions at $\sqrt{s} = 13$ TeV. JHEP **03**, 166 (2018). arXiv:1709.05406 [hep-ex]
224. ATLAS Collaboration, ATLAS searches for MSSM Higgs bosons decaying into SUSY cascades. ATL-PHYS-PUB-2009-079, ATL-COM-PHYS-2009-086 (2009)
225. M. Bisset, J. Li, N. Kersting, R. Lu, F. Moortgat, S. Moretti, Four-lepton LHC events from MSSM Higgs boson decays into neutralino and chargino pairs. JHEP **08**, 037 (2009). arXiv:0709.1029 [hep-ph]
226. C. Charlot, R. Salerno, Y. Sirois, Observability of the heavy neutral SUSY Higgs bosons decaying into neutralinos. J. Phys. G **34**, N1–N12 (2007)
227. C.M.S. Collaboration, G.L. Bayatian et al., CMS technical design report, volume II: physics performance. J. Phys. G **34**(6), 995–1579 (2007)
228. N. Craig, F. D'Eramo, P. Draper, S. Thomas, H. Zhang, The Hunt for the Rest of the Higgs Bosons. JHEP **06**, 137 (2015). arXiv:1504.04630 [hep-ph]
229. R.K. Barman, B. Bhattacherjee, A. Chakraborty, A. Choudhury, Study of MSSM heavy Higgs bosons decaying into charginos and neutralinos. Phys. Rev. D **94**(7), 075013 (2016). arXiv:1607.00676 [hep-ph]
230. S. Profumo, T. Stefaniak, L. Stephenson Haskins, The not-so-well tempered neutralino. Phys. Rev. D **96**(5), 055018 (2017). arXiv:1706.08537 [hep-ph]
231. P.S. Bhupal Dev, A. Pilaftsis, Maximally symmetric two Higgs doublet model with natural standard model alignment. JHEP **12**, 024 (2014). arXiv:1408.3405 [hep-ph] (**Erratum: JHEP 11, 147 (2015)**]
232. A. Pilaftsis, Symmetries for standard model alignment in multi-Higgs doublet models. Phys. Rev. D **93**(7), 075012 (2016). arXiv:1602.02017 [hep-ph]
233. I. Antoniadis, K. Benakli, A. Delgado, M. Quiros, A New gauge mediation theory. Adv. Stud. Theor. Phys. **2**, 645–672 (2008). arXiv:hep-ph/0610265
234. J. Ellis, J. Quevillon, V. Sanz, Doubling up on supersymmetry in the Higgs sector. JHEP **10**, 086 (2016). arXiv:1607.05541 [hep-ph]
235. K. Benakli, M.D. Goodsell, S.L. Williamson, Higgs alignment from extended supersymmetry. Eur. Phys. J. C **78**(8), 658 (2018). arXiv:1801.08849 [hep-ph]
236. S. Profumo, T. Stefaniak, Alignment without decoupling: the portal to light dark matter in the MSSM. Phys. Rev. D **94**(9), 095020 (2016). arXiv:1608.06945 [hep-ph]
237. G.H. Duan, W. Wang, L. Wu, J.M. Yang, J. Zhao, Probing GeV-scale MSSM neutralino dark matter in collider and direct detection experiments. Phys. Lett. B **778**, 296–302 (2018). arXiv:1711.03893 [hep-ph]
238. G.F. Giudice, A. Romanino, Electric dipole moments in split supersymmetry. Phys. Lett. B **634**, 307–314 (2006). arXiv:hep-ph/0510197
239. Y. Li, S. Profumo, M. Ramsey-Musolf, A comprehensive analysis of electric dipole moment constraints on CP-violating phases in the MSSM. JHEP **08**, 062 (2010). arXiv:1006.1440 [hep-ph]
240. Y. Nakai, M. Reece, Electric dipole moments in natural supersymmetry. JHEP **08**, 031 (2017). arXiv:1612.08090 [hep-ph]
241. A.C.M.E. Collaboration, V. Andreev et al., Improved limit on the electric dipole moment of the electron. Nature **562**(7727), 355–360 (2018)